醫學博士 學位論文

위축된 하지의 골격근동맥 수축성 및 이온통로기능에 대한 운동 훈련의 회복 효과

Restoration of skeletal artery contraction properties and ion channel functions by exercise training in unilateral hindlimb paralyzed rats

2019年 8月

서울大學校 大學院

醫科學科 醫科學專攻

尹 明 哲

A thesis of the Degree of Doctor of Philosophy

Restoration of skeletal artery contraction properties and ion channel functions by exercise training in unilateral hindlimb paralyzed rats

위축된 하지의 골격근동맥 수축성 및 이온통로기능에 대한 운동 훈련의 회복 효과

August, 2019

The Department of Biomedical Sciences,
Seoul National University College of Medicine

Ming Zhe Yin

위축된 하지의 골격근동맥 수축성 및 이온통로기능에 대한 운동 훈련의 회복 효과

Restoration of skeletal artery contraction properties and ion channel functions by exercise training in unilateral hindlimb paralyzed rats

지도교수 김 성 준

이 논문을 의학박사 학위논문으로 제출함

2019년 4월

서울대학교 대학원

의과학과 의과학전공

尹 明 哲

尹 明 哲의 의학박사 학위논문을 인준함

2019년 7월

위 원 장 _____ **(인)**

부위원장 _____ **(인)**

위 원 _____ **(인)**

위 원 _____ **(인)**

위 원 _____ **(인)**

Restoration of skeletal artery contraction properties and ion channel functions by exercise training in unilateral hindlimb paralyzed rats

by

Ming Zhe Yin

A thesis submitted to the Department of Biomedical Sciences in partial fulfillment of the requirements for the Degree of Doctor of Philosophy in Biomedical Sciences at Seoul National University College of Medicine

July, 2019

Approved by Thesis Committee:

Professor_____Chairman

Professor_____Vice chairman

Professor_____

Professor_____

Professor_____

ABSTRACT

Atrophic limbs exhibit decreased blood flow and histological changes in the arteries perfusing skeletal muscles. However, the effect of atrophy on vascular smooth muscle of skeletal artery function is poorly understood. Here, I investigated the effect of unilateral sciatic denervation on the myogenic response (MR) and the ionic currents in deep femoral artery (DFA) smooth muscles from Sprague–Dawley rats. Since denervated rats were capable of moderate treadmill exercise (20 m/min, 30 min, 3/week), the impact of exercise training on these effects was also assessed. Skeletal arteries were harvested 3 or 5 weeks after the surgery. Then, skeletal arteries or myocytes were subjected to video-analysis of pressurized artery, myography, whole-cell patch clamp, and RT-qPCR to determine the effect of hindlimb paralysis on MR, contractility, ionic currents, and TRPC channel transcription, respectively, in the presence of exercise training. In sedentary rats, atrophy was associated with loss of MR in DFA at 5 weeks. The contralateral DFA had a normal MR. At 5 weeks after surgery, DFA myocytes from the atrophic limbs exhibited depressed L-type Ca^{2+} currents ($I_{Ca,L}$), GTPγS-induced Transient Receptor Potential Canonical channel (TRPC)-like currents ($I_{GTP\gamma S}$), 80 mM KCl-induced vasoconstriction, TRPC6 mRNA, and voltage-gated K^+ and inwardly-rectifying K^+ currents. Exercise training abrogated the differences in all of these functions between atrophic side and contralateral side DFA myocytes by reversing the remodeling in atrophic side. These results suggest that

functions of MR changes were associated with ion channels in smooth muscle cell. This study provides evidence to support the patients with limb paralysis.

Keywords: Sciatic nerve, myogenic response, ion channel, smooth muscle, exercise training.

Student number: 2016-30781

CONTENTS

LIST OF FIGURES

Part I

Functional changes of skeletal arterial smooth muscle in denervated hindlimb of rats

Part II

Effects of endurance exercise on the skeletal artery functions in unilateral hindlimb atrophy rats

NONSTANDARD ABBREVIATIONS AND ACRONYMS

MR Myogenic Response

$I_{Ca,L}$ L-type Ca^{2+} channel current

I_{Kv} Voltage-gated K^+ channel current

I_{Kir} Inwardly rectifying K^+ channel current

I_{BKCa} Large-conductance Ca^{2+}-activated K^+ channel current

$I_{GTP\gamma S}$ GTPγS-activated current

TRPC Transient Receptor Potential Canonical channel

DFA Deep Femoral Artery

INTRODUCTION

1. Changes of skeletal arterial blood flow in paralyzed limbs.

Long-term immobilization of limbs due to causes such as denervation paralysis affects not only skeletal muscle but also the skeletal arteries that perfuse the corresponding sites (Thijssen et al., 2010). This is likely due to decreased blood flow. Indeed, *in vivo* studies of spinal cord injury patients show that blood flow to the paralyzed limbs is significantly lower than that in unaffected individuals (Hopman et al., 1996, 2002; Nash et al., 1996). This notion is supported by the original study showing that arterial diameter decreases when blood flow is reduced (Langille & O'Donnel, 1986). It is also supported by a recent review shows that arteries undergo remodeling when hemodynamics change. Structure adaptation remodeling of peripheral arteries occurs in paralyzed limbs soon after spinal cord injury; a consequent inward remodeling of the arterial wall, such that the diameter of the femoral artery is 30-50% smaller and resting blood flow in the leg is 30-40% lower than that in the contralateral part (West et al., 2013).

Several studies show that skeletal arteries in paralyzed limbs also undergo functional changes, including changes in flow-induced NO-mediated dilation and levels of vasoactive agents. These effects depend on the vessel type and conditions (Thijssen et al., 2010, 2012). However, most studies on skeletal artery function focused on endothelial function; the skeletal artery smooth muscle cells in motor

activity-deprived or paralyzed/atrophic limbs, especially their ion channel activity, have never been investigated directly.

2. Myogenic response of arteries and associated ion channels.

Of the various physiological functions of arterial smooth muscle, I chose to focus on the myogenic response (MR) of skeletal artery smooth muscle and the associated ion channel currents. MR refers to the reactive vasoconstriction and vasodilation that occurs when the transmural pressure increases and decreases, respectively (Kotecha & Hill, 2005; Tykocki et al., 2017). MR is an intrinsic property of resistance arteries, including small-diameter arteries feeding the skeletal muscles (Hill & Meininger, 2012; Kotecha & Hill, 2005). Experimentally, the MR of arteries are observed as a reactive vasoconstriction in response to the stepwise increases in the transmural pressure, and the small branches of skeletal arteries (SkA) also show MR (Kotecha & Hill, 2005; Baek et al, 2010).

Multiple mechanisms and factors interact to drive the MR. These include electrophysiological factors, as indicated by early reports showing that blood vessels undergo membrane depolarization when the transmural pressure increases (Harder, 1984; Hill & Meininger, 2012). Multiple lines of evidence suggest that of the various types of nonselective cation channel those could mediate the depolarization underlying MR, G-protein signaling-coupled transient receptor potential cation channels (TRPC) are most likely to be responsible (Hill-Eubanks et al., 2014;

Gonzales et al., 2014). It is likely that the mechanosensitive depolarization mediated by TRPCs activates the L-type Ca^{2+} current ($I_{Ca,L}$) in myocytes, which is counterbalanced by hyperpolarizing K^+ channel currents (Tykocki et al., 2017). In arterial myocytes, various types of K^+ channels contribute differently to this counterbalance depending on the cellular conditions and type of vessels (Tykocki et al., 2017). Of these, I here focus on three major K^+ currents in skeletal artery smooth muscle, namely, the voltage-gated K^+ channels (I_{Kv}), the inwardly-rectifying K^+ channels (I_{Kir}), and the large-conductance Ca^{2+}-activated K^+ channel current (I_{BKCa}).

3. Functional changes of skeletal artery by exercise training.

Skeletal blood flow to the contractile muscles increases dramatically in response to exercise, called exercise hyperemia (EH) (Saltin, 2017). Despite the increased sympathetic tone during exercise, the alpha-adrenergic constriction of skeletal arteries is effectively relaxed by the local metabolic signals and vasodilatory factors. Such functional sympatholysis during exercise leads to EH (Calbet & Lundby, 2012). Variety of vasodilatory mediators released from endothelium and skeletal muscles along with the muscle pump effects contribute to EH. One of the vasodilatory factors for EH is the moderate increase in extracellular K^+ concentration ($[K^+]_e$). Owing to K^+ release from contracting muscles with repetitive action potentials, the interstitial $[K^+]_e$ of muscular tissue increases up to 12 - 15 mM. Such moderate increase in $[K^+]_e$ effectively augments the activity of inwardly rectifying K^+ channels (Kir) of skeletal

arterial smooth muscle cells (SkASMCs), causing membrane hyperpolarization and arterial relaxation, called K^+-vasodilation (Crecelius et al., 2013; Juel et al., 2007).

In the present study, I also wanted to assess how exercise training affects the MR and ionic currents in skeletal artery myocytes. For that, I needed a suitable animal model. An early study reported that when the hindlimb of rats is unloaded (lifted), the MR in their skeletal muscle arterioles decreases (Delp, 1999). However, another study of hindlimb-unloaded rats found that the spontaneous tone of the skeletal artery either rose or remained unaltered; which of these occurred apparently depended on the supplying muscle types (Heaps & Bowles, 2002). This discrepancy suggests that the hindlimb-unloaded rodent model may not be suitable for our study. This model is also not suitable because the long-term hindlimb lifting condition might impose various systemic effects and stress on the animals. Moreover, it is technically difficult to apply other conditions such as exercise training. Therefore, I adopted the unilateral hindlimb paralysis rat model, where one sciatic nerve is severed under anesthesia. This model is technically simple and consistently induces atrophy of the lower hindlimb.

Another advantage of the unilateral paralysis model for our study is that I could compare the affected and intact contralateral skeletal arteries in terms of MR and ionic currents; thus the contralateral skeletal artery was used as an internal sham surgery control. Furthermore, our pilot experiment showed that despite the paralysis of one hindlimb, the model rats could perform a moderate level of treadmill exercise by using

the other intact legs (see Methods). This meant that the model was suitable for elucidating the effect of endurance exercise training during paralysis on the functions of the skeletal artery of the paralyzed hindlimb.

Repetitive exercise training, particularly endurance training, induces functional remodeling of systemic arteries (Green et al., 2012, 2017; Jin et al., 2011; Seo et al., 2014). However, it is not known whether exercise training affects the MR and ionic currents in the skeletal arteries of a paralyzed/atrophic limb. Based on previous observations that endurance exercise increases the K^+ current density of skeletal arterial myocytes (Jin et al., 2011; Seo et al., 2014), I hypothesized that unilateral hindlimb paralysis might selectively lower the ion channel activity of the arteries on the affected side. Furthermore, since the skeletal muscles of the paralyzed limb would not effectively show exercise-induced hyperemia when compared with those of the intact limb, it is supposed that functional changes in skeletal arteries on the atrophic side might be different from those on the contralateral side. By contrast, if exercise-mediated effects on skeletal arteries are mediated by systemic factors, or by overall increases in hemodynamic stimuli, then functional changes might be observed in arteries on the atrophic side. These questions were addressed in the present study.

Thus, the present study provides clues with electrophysiological data that will help us to better understand the pathophysiological changes in human skeletal arteries in paralyzed or atrophied limbs after sports injury or accident. Our findings also help us

to understand, for the first time, the rehabilitative effects of exercise training on limb paralysis at the level of smooth muscle electrophysiology.

MATERIALS & METHODS

Animals models and tissue samples

The study protocol was in accordance with the 'Guide for the Care and Use of Laboratory Animals' published by the US National Institutes of Health (NIH Publication Eighth edition, revised 2011), and also conformed to Institutional Animal Care and Use Committee (IACUC) in Seoul National University (IACUC approval No.: SNU-150203-3-1). Sprague–Dawley rats (8 weeks old, male) were randomly assigned to either a sciatic nerve severed sedentary group (i.e. without exercise training, n = 84) or exercise training group (n = 82). The sciatic nerve denervation surgery was performed under deep anesthesia using isoflurane. Thereafter, the rats were randomly assigned to either the sedentary control or exercise training group. After one week of recovery period, the exercise training group rats were trained to perform motor-driven treadmill running (20 m/min for 30 min without inclination, 3 times/week) for two or four weeks (Fig. 1A). Despite the paralysis and atrophy of the unilateral lower hindlimb, the rats could perform the treadmill running protocol using the intact legs. Also, it was notable that the sciatic nerve injured leg still showed

outwardly swaying movement during the running process with the gluteal and thigh muscles that were not paralyzed. The sedentary control and exercise training group rats were sacrificed at either three or five postoperative weeks. Thus, there were four groups (3w, 5w, 3w/ET-2w and 5w/ET-4w, Fig. 1A) of rats. For the measurement of MR, the sedentary rats were also sacrificed 1 week after surgery.

To get tissue samples, the rats were anesthetized with injection of ketamine and xylazine mixture (ketamine 90 mg/kg and xylazine 10 mg/kg, i.p. injection) and were immediately killed by decapitation after confirming a fully anaesthetized state. The gastrocnemius muscles were isolated and moved to NT solution containing (in mM/L) 140 NaCl, 5.4 KCl, 0.33 NaH_2PO_4, 10 HEPES, 10 Glucose, 1 $CaCl_2$, and 1 $MgCl_2$, adjusted to pH 7.4 with NaOH. DFAs feeding the lower hindlimb muscles were dissected under stereomicroscope (Fig. 1C), and prepared for the contraction study or single myocyte isolation. To analyze the atrophic state of denervated muscles, the weight of gastrocnemius and tibialis posterior muscle were compared in each group of the model animals (Fig. 2A).

Isometric tension recording with dual-wire myograph

Dissected DFA lying exterior to muscle (i.e. feeding arteries located between adductor magnus and gastrocnemius) were prepared with length of 3 mm and mounted on 25 μm tungsten wires for measurement of isometric tone using dual-wire myograph

system (620 M; DMT, Aarhus, Denmark). The chambers were filled with physiological salt solution (PSS) containing (in mM/L) 118 NaCl, 4 KCl, 0.44 NaH_2PO_4, 24 $NaHCO_3$, 1 $MgSO_4$, 5.6 glucose, and 1.8 $CaCl_2$. The PSS was equilibrated with gas bubbling (21 % O_2, 5 % CO_2, balanced N_2) and the temperature was maintained at 37 °C. The viability of each artery was evaluated from contraction induced by 80 mM KCl solution (80K-contraction) where the equivalent amount of NaCl was substituted with KCl.

Video analysis of pressurized arteries

Dissected DFA segments were placed in a glass-bottomed vessel chamber (Model CH/1/SH; Living Systems Instrumentation, Burlington, VT, USA). The vessel chamber contained NT solution. The temperature of the vessel chamber set at 37-38 °C using a controller (Model TC-01; Living Systems Instrumentation). The vessels were cannulated using glass micropipettes and secured with 12–0 nylon suture. There was almost no luminal flow during the experiment measuring the luminal diameter (D_{in}) of cannulated artery. The value of luminal pressure (P_{lum}) was set to 60 mmHg for at least an additional 40 min; spontaneous increase in myogenic response developed in more than 90 % of DFAs from normal control rats. After confirming the stable myogenic response, P_{lum} was lowered to 20 mmHg for 15 min, and stepwise increases of P_{lum} to 120 mmHg was applied. D_{in} was initially increased (initial passive dilation) and then decreased, which reflects active myogenic responses (MR). To

quantify MR of arteries, the maximal passive diameter ($D_{max,0Ca}$) was measured in Ca^{2+}-free NT solution (0Ca-NT) with 1 mM EGTA. The maximal increase in D_{in} (ΔD_{max}) by changing to the 0Ca-NT was divided by $D_{max,0Ca}$ ($\Delta D_{max}/D_{max,0Ca}$), resulting the MR (%) at each P_{lum}.

Single cell isolation and patch clamp recording

After the dissection of arteries, vessels were incubated in the first digestion medium (nominal Ca^{2+}-free NT solution containing 1mg/mL papain) for 10-15 min, and changed to the second digestion medium (nominal Ca^{2+}-free NT solution containing 3 mg/mL collagenase) for another 10-15 min. Both digestion media contained bovine serum albumin (1 mg/mL) and dithiothreitol (1 mg/mL). The isolated smooth muscle cells were suspended with a polished wide pipette and stored in a K^+-rich solution that contained (in mM/L): 70 KOH, 50 L-glutamate, 55 KCl, 20 taurine, 20 KH_2PO_4, 3 $MgCl_2$, 20 Glucose, 10 HEPES, and 0.5 EGTA, adjusted to pH 7.3 with KOH.

Whole-cell patch clamp experiments were performed with a patch clamp amplifier (Axopatch-200B, Axon Instruments, Foster City, CA, USA). The pCLAMP software 10.4 and Digidata-1550A (Axon Instruments) were used to acquire data and apply command pulse. Currents recording were performed at room temperature (23-25 °C). Glass microelectrode with a resistance of about 2.2-2.5 MΩ were used. The electrical capacitance was measured in each cell (Fig. 5A, B), and used to normalize the current

amplitude, i.e. current density (pA/pF).

The pipette solution for recording GTPγS-activated nonselective cation channel current ($I_{GTP\gamma S}$) contained (in mM/L) 145 CsCl, 10 EGTA, 10 HEPES, 0.3 mM GTPγS, 3 Mg-ATP and 1 $MgCl_2$, adjusted to pH 7.2 with CsOH. The bath solution contained (in mM/L) 145 CsCl, 1 $CaCl_2$, 10 HEPES, 1 $MgCl_2$, 10 Glucose adjusted to pH 7.2 with CsOH. The pipette solution for recording $I_{Ca,L}$ contained (in mM/L) 130 CsCl, 10 HEPES, 5 Mg-ATP, 10 EGTA, 2 $MgCl_2$, 2 Na_2-GTP, 12 NMDG-Cl adjusted to pH 7.2 with CsOH. The bath solution for recording $I_{Ca,L}$ contained (in mM/L) 140 CsCl, 10 $BaCl_2$, 10 HEPES, 10 Glucose, 4.7 KCl adjusted to pH 7.4 with CsOH.

The Ca^{2+}-free pipette solution for recording I_{Kv} and I_{Kir} contained (in mM/L) 20 KCl, 120 K-aspartate, 10 HEPES, 1 $MgCl_2$, 3 MgATP (adenosine 5′-triphosphate), 10 EGTA, adjusted to pH 7.2 with KOH. The pipette solution for recording I_{BKCa} contained (in mM/L) 20 KCl, 120 K-aspartate, 10 HEPES, 1 $MgCl_2$, 3 MgATP, adjusted to pH 7.2 with KOH, and free Ca^{2+} activity was clamped to 10 μM using 10 mM HEDTA and $CaCl_2$ according to WinMAX (Chris Patton, Stanford University, http://www.stanford.edu/~cpatton/maxc.html). I_{Kv} and I_{BKCa} were recorded in the NT bath solution. To maximally reveal the density of I_{Kir}, the symmetric high K^+ solution-140 mM KCl bath solution (140K solution) was used that contained (in mM/L): 140 KCl, 10 HEPES, 10 Glucose, 1 $CaCl_2$, and 1 $MgCl_2$ adjusted to pH 7.4 with NaOH. At the currents detecting steady state, gave the 100 μM $BaCl_2$ to block of the inward

current component, calculation of the selective of the density of I_{Kir}.

Histology

Isolated DFAs with perivascular tissues were fixed in 4% paraformaldehyde and embedded in paraffin. For histological analysis, tissue sections were cut at 5 μm and stained with Masson's trichrome staining kit according to the manufacturer's instructions (HT15-1KT, Sigma Aldrich, St. Louis, MO, USA). Images of stained tissues were taken using Leica microsystems and LAS 4.0 software (Leica, Germany) with a 20x objective. Images were analyzed by Adobe photoshop CC software to measure the relative areas of the vascular lumen and media.

RNA extraction and real time quantitative PCR

Total RNA was extracted from isolated DFA myocytes using TRIzol reagent (Invitrogen, Carlsbad, CA, USA) method according to the instruction. mRNA was reverse transcribed by standard reaction using cDNA synthesis Master Mix (Takara Bio Inc, Japan). Specific rat primers for TRPC3, 4, 6 and α-actin were as follows: TRPC3 (accession number: NM_021771) (forward, 5'-GAGATCTGGAATCGGTGGAA-3'; reverse, 5'- AAAAGCTGCTGTTGGCAGTT-3'), TRPC4 (accession number: NM_053434) (forward, 5'-

GACACGGAGTTCCAGAGAGC-3'; reverse, 5'-GTTGGGCTGAGCAACAAACT-3'), TRPC6 (accession number: NM_053559) (forward, 5'-TACTGGTGTGCTCCTTGCAG-3'; reverse, 5'-GAGCTTGGTGCCTTCAAATC-3'), β-actin (accession number: NM_031144) (forward, 5'- TAAGGCCAACCGTGAAAAGATG-3'; reverse, 5'-GTACGACCAGAGGCATACAGG-3'). PCR was performed with 2X Taq premix (SolGent, Deagon, Korea) using a DNA thermal cycler (Bio-Rad Laboratories, Hercules, CA, USA) to confirm the expression of TRPC3, 4, 6 mRNA. cDNA was quantified with real-time quantitative PCR in an CFX Connect^{TM} Real-Time PCR Detection System (Bio-Rad Laboratories, Hercules, CA, USA). The qPCR reaction was performed using HiPi Real-Time PCR 2x Master Mix SYBR green (ELPis, Taejeon, Korea). In a final mixture volume of 20 μl. The program of real-time qPCR consisted of three steps including a hot holding stage at 95 °C for 10 min, 40 cycles with each containing 95 °C for 15 s, 60 °C for 1 min, and melting curves performed at 95 °C for 15 s, 60 °C for 1 min. Triplicate measurement were calculated using the relative standard curve method. Data were expressed as a relative expression levels assessed using the comparative threshold (C_t) values according to the $2^{-\Delta\Delta Ct}$ methods (Livak & Schmittgen, 2001).

Chemicals

All drugs and chemicals were obtained from Sigma-Aldrich (St. Louis, MO, USA).

Statistical analyses

Data were presented as means ± SEM with the number of tested cells for the patch clamp study or the number of tissues for the myograph are indicated as *n*. The numbers of animals for each study are also indicated in the corresponding figure legend. Data were analyzed using two-group Student's t-test, which included one within-subject factor (contralateral side and atrophic side). For the multiple comparisons of two-group (e.g. atrophy and contralateral side DFA from sedentary and exercise training groups), two-way ANOVA followed by post-hoc Bonferroni were applied (Fig. 6). Statistically significant differences were defined as $p < 0.05$. In the figures, *, ** and *** indicate $p < 0.05$, 0.01, and 0.001 respectively.

RESULTS

Part I

Functional changes of skeletal artery smooth muscle in denervated hindlimb of rats

Sciatic nerve anatomy and preparation of the sciatic denervation rat model.

The sciatic nerve is a large nerve in the human and animals, derived from spinal cord nerves L4 to S3 formed the sacral plexus, which largely comprises of motor neuron axon and some sensory nerve fibers for the posterior thigh, most of the lower limb and foot (Fig. 1B). The sciatic nerve denervation surgery was performed under deep anesthesia using isoflurane (Fig. 1C, left image). In all four groups, the paralyzed hindlimb became atrophied, characterized by a clawed foot and wasted appearance by 3 weeks post-surgery (Fig. 1C, right image). Dissection of the DFAs at 5 weeks showed that the muscle mass decreased and the perivascular soft tissue increased (Fig. 1D). The body weights (g) in Fig. 1E were not significantly different between sedentary and exercise training groups of the same age matched S-D rats; 3w (354±6.4, n=17) *vs.* 3w/ET-2w (359±6.2, n=17), and 5w (383±4.9, n=20) *vs.* 5w/ET-4w (387±3.8, n=20).

Decrease of gastrocnemius and tibialis posterior muscles in the sciatic nerve denervated limb.

To confirm the denervation model, we measured the sciatic nerve denervation side muscle masses compared with the contralateral side. I then dissected and weighed the gastrocnemius and tibialis posterior muscles in all groups. As can be seen in Figure 2A, the sciatic-denervated limbs had significantly lower gastrocnemius and tibialis posterior muscle weights than the contralateral limbs in all groups (muscle weight, g, 1w contralateral side gastrocnemius 0.7±0.03 n=10 *vs* Atr gastrocnemius 0.4±0.02 n=10; 1w contralateral side tibialis posterior 0.4±0.01 n=10 *vs* Atr tibialis posterior 0.2±0.01 n=10; 3w contralateral side (CL) gastrocnemius 0.9±0.01 n=18 *vs.* Atrophic side (Atr) gastrocnemius 0.3±0.01 n=18; 3w contralateral side tibialis posterior 0.4±0.01 n=18 *vs.* Atrophic side tibialis posterior 0.1±0.01 n=18; 5w contralateral side gastrocnemius 1.0±0.02 n=13 *vs.* Atrophic side gastrocnemius 0.3±0.02 n=13; 5w contralateral side tibialis posterior 0.4±0.01 n=13 *vs.* Atrophic side tibialis posterior 0.1±0.01 n=13).

Structural changes in the DFAs of the atrophic side.

To check whether the atrophic side skeletal arterial structure changes in the sciatic nerve denervation model, the atrophic side and contralateral side DFAs were compared in terms of structural changes by cross-sectional microscopy of Masson's trichrome stained tissue (Fig. 3A, B). The total area of outer medial border (Total) and

lumen area (Inner) wall area (Total-lumen) were measured by image analysis (Fig. 3C-E, respectively). In the sedentary hindlimb-atrophy rats, the atrophic DFAs have a statistically smaller total area than the contralateral DFAs groups at 5 postoperative weeks. Similar observations were made with the medial and wall area data. The lumen and wall area data of the sedentary rat, the atrophic side arteries tended to have a smaller area than the contralateral in 3 postoperative weeks and significance smaller at 5 postoperative weeks.

Atrophy side arteries exhibit a drop in MR at 5 postoperative weeks.

To assess the effect of paralysis on the MR of the DFA, the lumens of the dissected arteries were placed under various degrees of pressure (P_{lum}) and their dilation (D_{in}) was subjected to video-analysis. As the P_{lum} increased in a stepwise fashion from 20 to 120 mmHg, the contralateral DFAs of all rats exhibited initial passive dilation followed by contractile responses (Fig. 4A, B). These responses were more prominent at higher pressure ranges. These pressure increase-induced contractile responses represent the MR of the vessel. Analysis of sedentary rats that were sacrificed 1, 3, and 5 weeks after surgery showed that the atrophic and contralateral DFAs of the first postoperative week rats (1w) had similar MR (Fig. 4C-E). At the third postoperative week, the MR of the atrophic DFA appeared to be attenuated at higher pressures (>80 mmHg). However, it did not achieve statistical significance (Fig. 4D). By the fifth

week after surgery, the MR of the atrophic DFA was largely abolished, and differed significantly from the contralateral artery at all pressures except the two lowest (Fig. 4B, E). Consistent with the loss of MR, at the transmural pressure of 80 mmHg under NT solution, the D_{in} of atrophic DFA was larger than those of contralateral arteries by the fifth week after surgery (Fig. 4F). In contrast, the D_{in} under 0Ca-NT solution was not different between atrophic and contralateral DFAs (Fig. 4G).

Changes of inward cationic currents in the atrophic side DFA smooth muscle cell.

Since atrophy consistently associated with the disappearance of MR in the sedentary rats, the ionic currents of the DFA myocytes were examined. The ionic currents of the DFA myocytes were measured from the sedentary 3w and 5w rats by the whole-cell patch clamp analysis. Current amplitude was divided by membrane capacitance measured in each cell to provide current density value (pA/pF). It was notable that the electrical capacitances of DFA myocytes from the atrophy side were slightly lower than those of the contralateral side myocytes (Fig. 5A, B).

The TRPC currents in DFA myocytes were obtained from sedentary 3w and 5w rats. This analysis was performed by dialyzing the cells with GTPγS in the CsCl pipette solution. The bath solution was also composed of CsCl to exclude K^+ conductance. It is well known that GTPγS permanently binds with the alpha-subunit

of G proteins, thereby activating the G-protein-dependent TRPC channels (Abramowitz 2009, Seo 2014). After the membrane break-in for whole-cell recording, the intracellular dialysis with GTPγS slowly activated the inward current ($I_{GTP\gamma S}$) at -10 mV of holding voltage. It was confirmed that 10 μM Gd^{3+} completely inhibited $I_{GTP\gamma S}$ in each cell (Fig. 6C). The current-voltage relation (I/V curve) of $I_{GTP\gamma S}$ was obtained by reverse-ramp pulse from 100 to -140 mV. The weakly outward rectifying I/V curve with 0 mV of reversal potential suggested nonselective permeability of the activated channels (Fig. 6A, B). The current density of Gd^{3+}-sensitive $I_{GTP\gamma S}$ at -60 mV was significantly lower in both obtained from 3w and 5w atrophic DFA myocytes than the corresponding contralateral DFA myocytes (Fig. 6D).

I then analyzed the $I_{Ca,L}$ of the myocytes was measured by using 10 mM Ba^{2+} as the charge carrier. Membrane voltage was maintained at -50 mV and step-like depolarizing pulses ranging from -50 to 50 mV were applied with 10 mV intervals. The inward currents that were activated from above -40 mV were abolished by 1 μM nifedipine, an L-type Ca^{2+} channel blocker (Fig. 7B, inset). The atrophic DFA myocytes consistently showed a smaller $I_{Ca,L}$ than contralateral DFA myocytes (Fig. 7A, B). The peak amplitudes of $I_{Ca,L}$ density were then plotted against the test voltages to obtain the current-voltage relation (I/V curve) of $I_{Ca,L}$. In the sedentary 3w and 5w, the averaged I/V curves show that the atrophic DFA myocytes had a significantly lower $I_{Ca,L}$ density (pA/pF) than the contralateral DFA myocytes (Fig. 7C, D).

Vasocontractility were attenuated in the DFAs of atrophic side.

Along with patch clamp technique, high concentration KCl-induced vasocontractility was evaluated using wire myography to indirectly test that atrophy attenuates myogenic constriction by reducing the currents of L-type voltage-dependent Ca^{2+} channels. I used 80 mM high-K^+ solution compared the atrophic side and contralateral DFA contractility (Fig. 8A, B). In the sedentary 3w, there were no significant differences of high-K^+ (80mM) induced contraction between contralateral side and atrophic side (Fig. 8A). Interestingly, consistent with the lower $I_{Ca,L}$, the atrophic DFAs exhibited lower high-K^+ (80 mM)-induced contraction than the contralateral DFA in sedentary 5w (Fig. 8B).

To investigate the changes in α-adrenergic receptor agonist induced vasoconstriction, I used phenylephrine (PhE, selectively binds to alpha-1 receptors) which cause artery contraction. Using dual-wire myography, isometric tension by 5 μM PhE were compared between the DFA from atrophic side and contralateral side hind limbs. In the sedentary 3w, the contractility of induced by 5 μM PhE were no difference between contralateral side and atrophic side (Fig. 8C). By contrast, with PhE induced vasoconstriction significantly attenuated from the atrophic side DFA compared to contralateral side DFA in the sedentary 5w (Fig. 8D).

Changes of K^+ channel currents density in DFA smooth muscle cells of atrophic side in sedentary rats

The voltage-gated K^+ channel current (I_{Kv}) in DFA myocytes from 5w was measured by using 10 mM EGTA-KCl pipette solution and NT bath solution. The brief I/V curves obtained by depolarizing ramp pulses from -80 to 60 mV was repetitively applied at every 10s. During inter-pulse period, the cell membrane voltage was hold at voltage -80 mV showed outward rectification that is consistent with the voltage-dependent activating property of Kv channels. The amplitude of the outward current was not affected by the BK_{Ca}-selective inhibitor paxilline (1 μM) but was significantly decreased by 1 mM of 4-aminopyridine (4-AP, Fig. 9A). The myocytes from the atrophic DFAs from 3w or 5w had significantly lower current densities of I_{Kv} at 40 mV than the contralateral DFA myocytes (Fig. 9B).

To record I_{BKCa}, the free Ca^{2+} activity in the KCl pipette solution was clamped to 10 μM and the holding voltage was set at -20 mV to inactivate I_{Kv}. Under this condition, the current response to hyperpolarizing ramp pulse from 60 to -80 mV showed a large outward current that was almost completely inhibited by 1 μM paxilline (Fig. 9C). While the myocytes from the atrophic DFAs in sedentary rats at 3 or 5 postoperative weeks tended to exhibit higher I_{BKCa} density than the myocytes

from the contralateral DFAs, this difference did not achieve statistical significance (Fig. 9D).

I_{Kir} was recorded with a high EGTA pipette solution and a high KCl bath solution, *i.e.,* a symmetrical K^+ condition, to reveal the inward current component of I_{Kir} (Fig. 10E, inset). Depolarizing ramp pulses from -100 to 60 mV were applied to obtain I/V curves. The inward K^+ current component was selectively abolished by 100 μM Ba^{2+}, a Kir channel blocker, added to the bath solution. The Ba^{2+}-sensitive current was obtained by digital subtraction in each cell, which revealed inwardly-rectifying I/V curves (Fig. 9E). The myocytes from atrophic DFAs in sedentary rats at 3 postoperative weeks had lower I_{Kir} densities than the myocytes from the contralateral DFAs and in 5 postoperative weeks, the differences achieve more statistical significance (Fig. 9F).

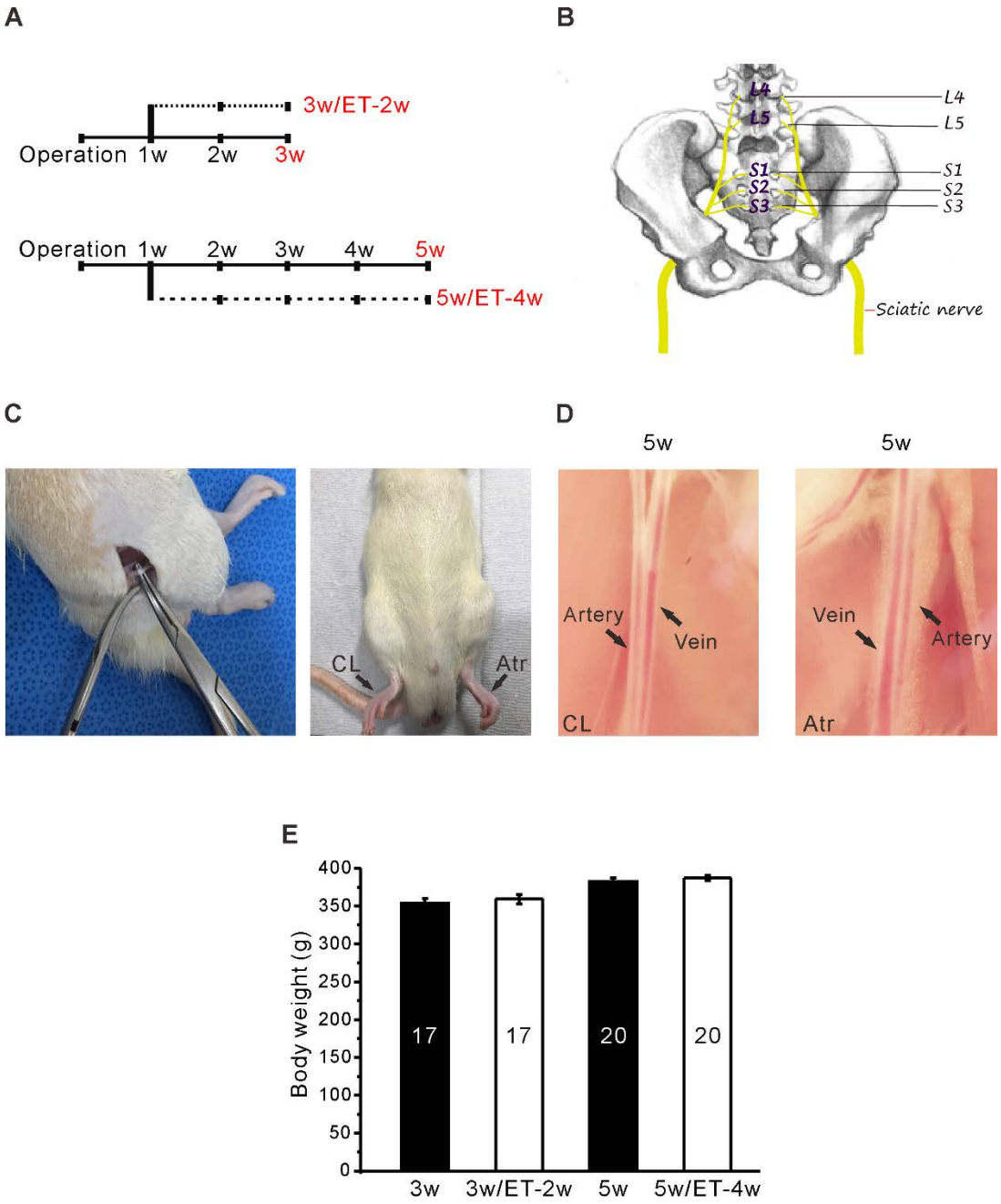
A
3w/ET-2w
Operation 1w 2w 3w
Operation 1w 2w 3w 4w 5w
5w/ET-4w
B
L4
L5
S1
S2
S3
Sciatic nerve
C
CL
Atr
D
5w
5w
Artery
Vein
CL
Vein
Artery
Atr
E
Body weight (g)
400
350
300
250
200
150
100
50
0
17
17
20
20
3w
3w/ET-2w
5w
5w/ET-4w

Figure 1. Preparation process of sciatic nerve paralysis model

(A) Schedule of denervation (Operation) and exercise training. The names of the experimental groups are indicated in red: sedentary 3 weeks after operation (3w); sedentary 5 weeks after operation (5w); 2 weeks of exercise training (ET)-combined 3w (3w/ET-2w); and four weeks of ET-combined 5w (5w/ET-4w). (B) Anatomy of sciatic nerve, the sciatic nerve originates from spinal cord L4-S3, (C) Sciatic nerve surgery (left) and appearance of the hindlimb at Week 3 post-op (right). (D) Appearance of vessels in atrophic (Atr) and contralateral (CL) hindlimbs of a rat in the 5w group (E) Summary of body weight in 4 group.

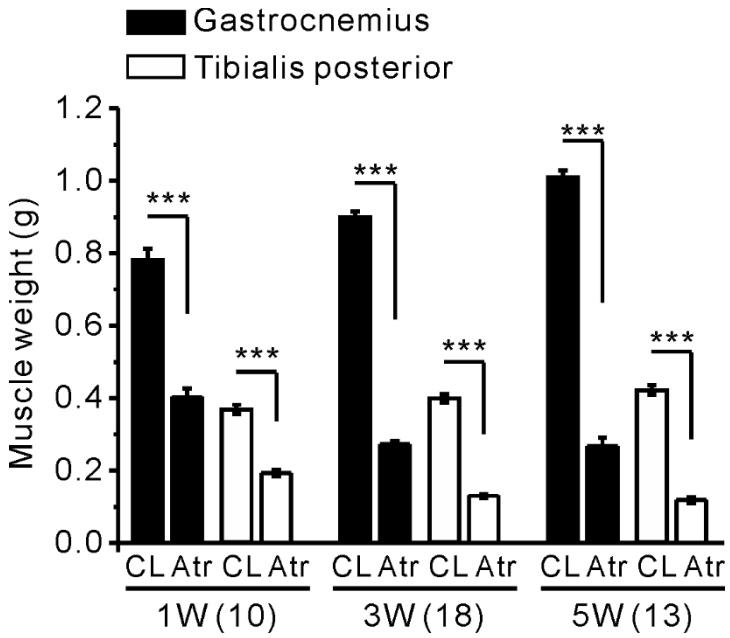

Figure 2. Hindlimb muscle atrophy in unilateral sciatic denervation model.

Summarized wet weights of gastrocnemius and tibialis posterior muscle obtained from CL and Atr hindlimbs in 1w (first week after operation), 3w (sedentary three weeks after operation) and 5w (sedentary five weeks after operation) rats. The gastrocnemius and tibialis posterior muscle weights were significantly smaller in Atr than CL (means ± SEM, ***$P < 0.001$, paired Student's *t* test).

A


3w, CL
100 μm
3w, Atr
100 μm

B


5w, CL
100 μm
5w, Atr
100 μm

C

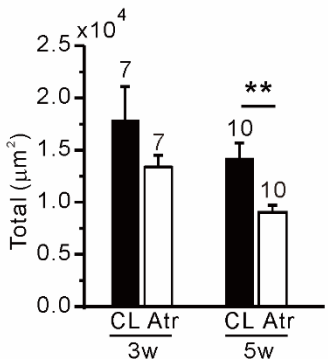
x10^4
Total (μm^2)
2.5
2.0
1.5
1.0
0.5
0.0
7
7
10
10
**
CL Atr
3w
CL Atr
5w

D

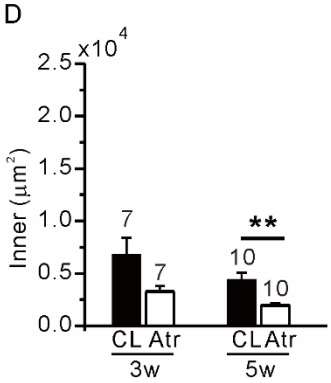
x10^4
Inner (μm^2)
2.5
2.0
1.5
1.0
0.5
0.0
7
7
10
10
**
CL Atr
3w
CL Atr
5w

E

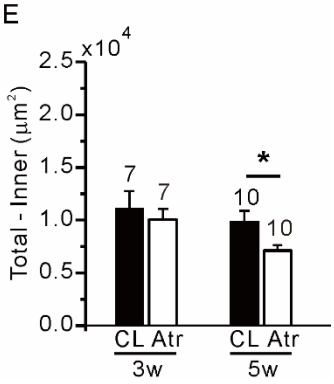
x10^4
Total - Inner (μm^2)
2.5
2.0
1.5
1.0
0.5
0.0
7
7
10
10
*
CL Atr
3w
CL Atr
5w

Figure 3. Comparisons of structural changes in atrophic and contralateral DFAs by Masson's trichrome stained tissue.

(A, B) Representative images showing Masson's trichrome staining of the atrophic side and contralateral side DFA from 3w and 5w. Summary of total outer medial area (Fig. 3C), luminal area (Fig. 3D) and medial wall area (Fig. 3E, Total-lumen). At 3-weeks post-surgery rats, the areas of total, inner and total-lumen were no statistical significantly difference between atrophic side DFAs and contralateral side DFAs, while sedentary 5 weeks after operation the atrophic side were smaller than the contralateral side. The number of samples are indicated upper of each bar (means ± SEM, $*P < 0.05$, $**P < 0.01$, paired Student's *t* test).

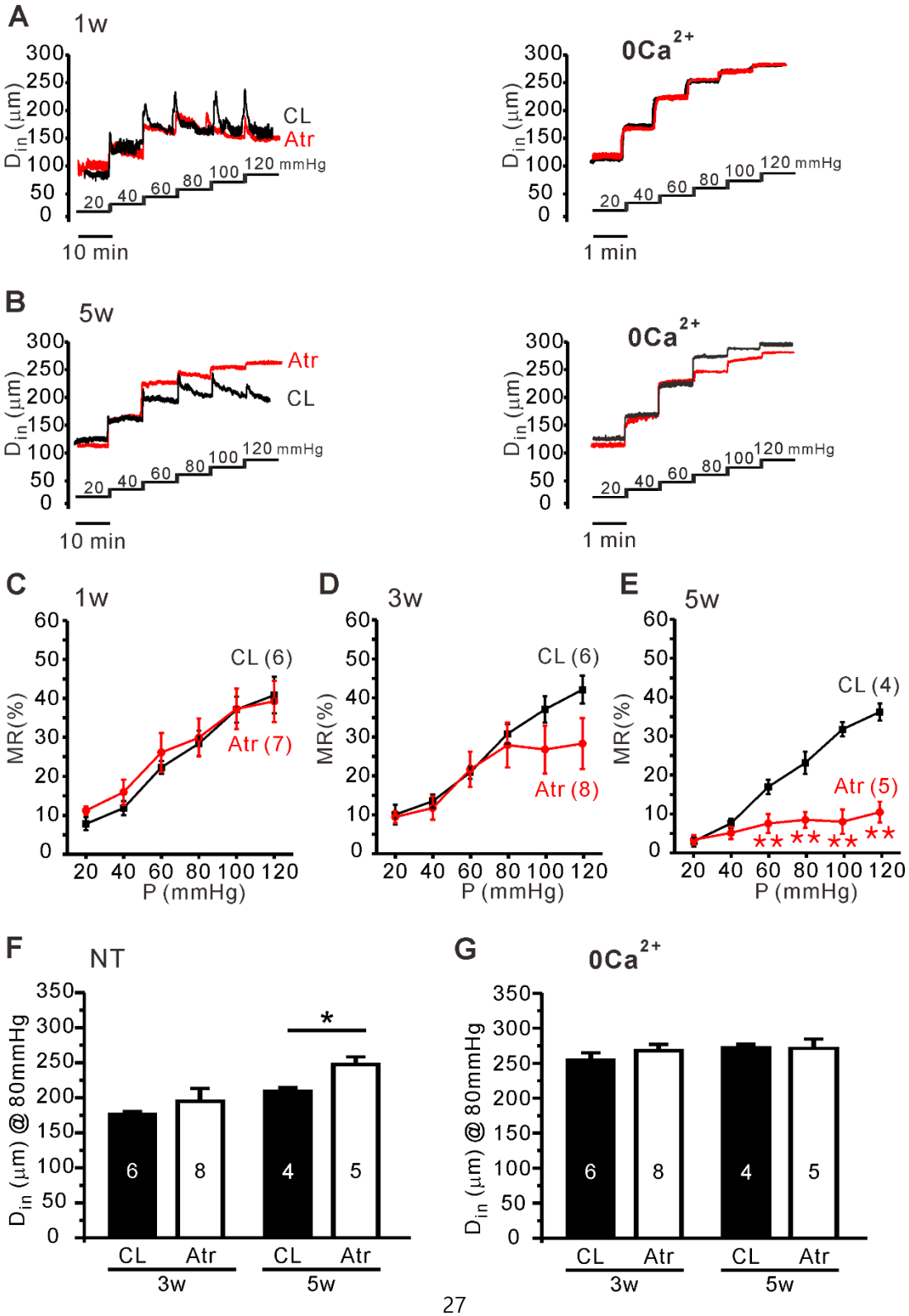
A
1w
0Ca2+
CL
Atr
20 40 60 80 100 120 mmHg
10 min
1 min
B
5w
C
1w
D
3w
E
5w
CL (6)
Atr (7)
Atr (8)
CL (4)
Atr (5)
MR(%)
P (mmHg)
F
NT
G
0Ca2+
Din (μm) @ 80mmHg
6
8
4
5
CL
Atr
3w
5w

Figure 4. Decay of MR in the DFA on the atrophic side.

(A, B) Representative trace of D_{in} in response to stepwise increases in P_{lum} in contralateral (CL, black) and atrophic side (Atr, red) DFAs at 1 week (1w, A) and 5 weeks (5w, B) post-surgery. (C–E) Summary of the MR (%, see *Methods*) for the CL and Atr at each P_{lum} in 1w (C), 3w (D), and 5w (E) rats. Note that the MR of the atrophic-side DFA disappeared in 5w rats. The number of DFA samples and animals was the same and is indicated in parentheses. (F, G) Summary of D_{in} at 80 mmHg of P_{lum} in DFAs from 3w and 5w rats under NT and Ca^{2+}-free ($0Ca^{2+}$) conditions (means ± SEM, $*P < 0.05$, $**P < 0.01$, unpaired Student's *t* test).

A

	Post-op, 3w Cell capacitance (pF)		Post-op, 5w Cell capacitance (pF)	
	CL	Atr	CL	Atr
Sed	24.3±0.60 (n = 87)	22.0±0.75 * (n = 66)	25.5±0.53 (n = 95)	23.9±0.69 * (n = 87)
ET	24.6±0.82 (n = 52)	25.3±0.79 (n = 47)	26.9±0.69 (n = 83)	26.0±0.65 (n = 95)

B

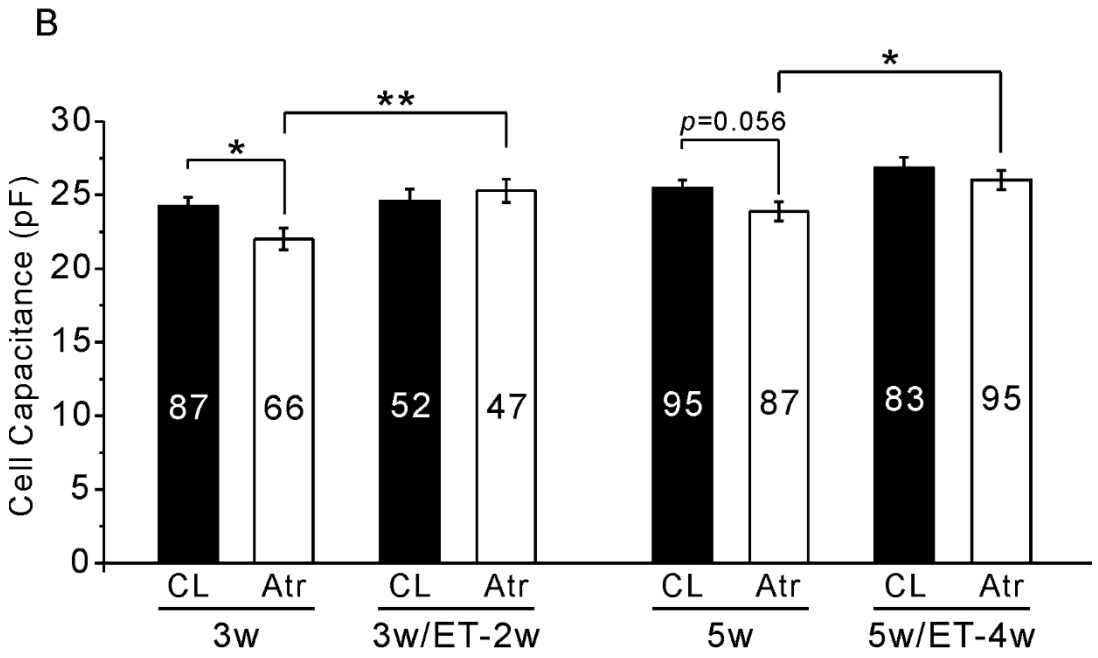

Figure 5. Comparison of atrophic and contralateral DFA smooth muscle cell capacitance in sedentary and sedentary combined ET rats.

(A) Summary of DFA smooth muscle cell membrane capacitance measured by whole-cell patch clamp analysis. The cell membrane capacitance obtained at atrophic side DFA were smaller than contralateral side in sedentary group, while similar size was detected in the sedentary combined rats group. (B) To clearly see the changes tendency of cell membrane capacitance, the data indicated in bar graph. The number of samples are indicated in the table and each bar. Values are expressed as means ± SEM. * $P < 0.05$. Abbreviations: CL, Contralateral deep femoral arterial myocytes; Atr, Atrophic deep femoral arterial myocytes; Sed, Sedentary; ET, Exercise training.

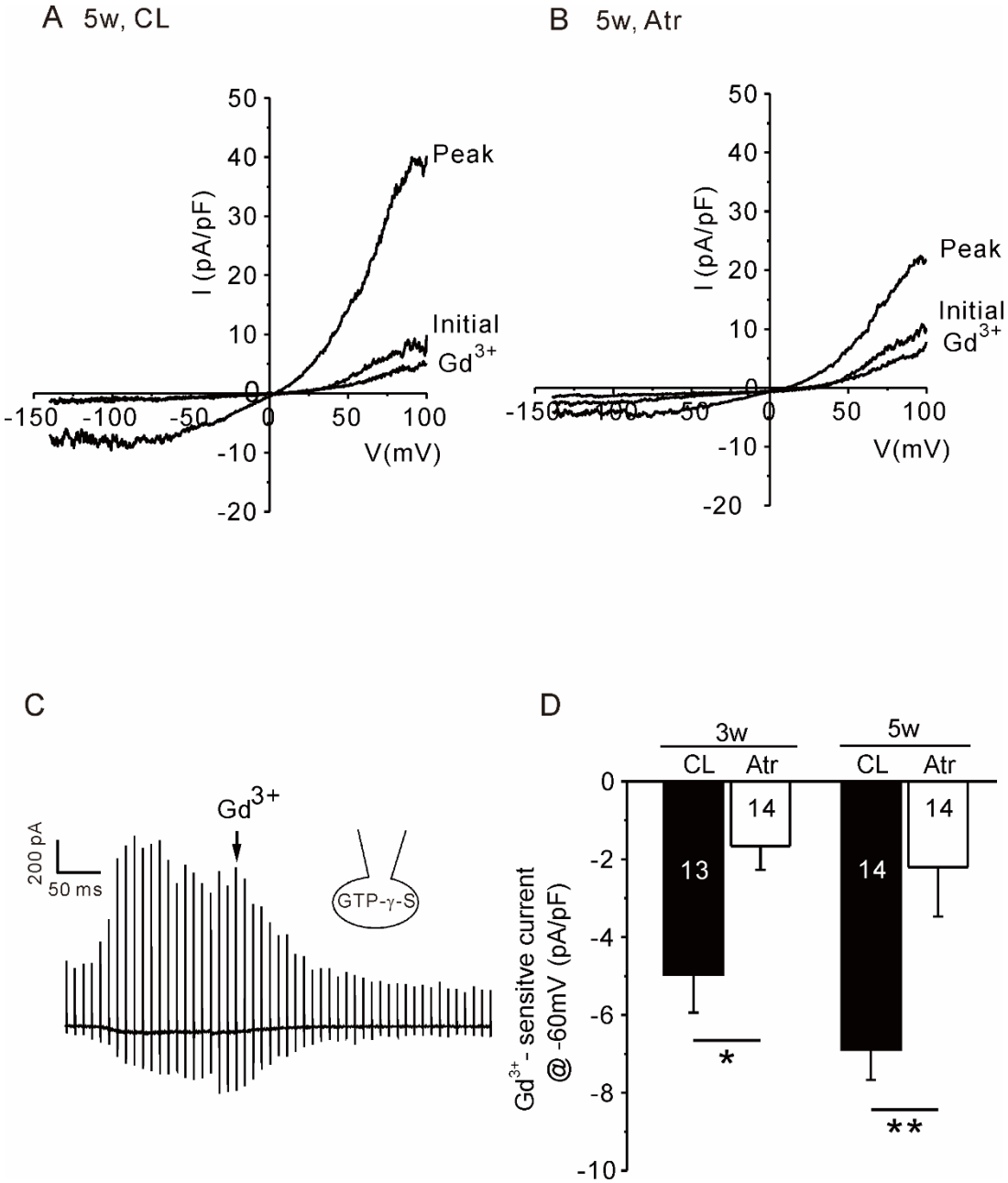
A 5w, CL
B 5w, Atr
I (pA/pF)
V(mV)
Peak
Initial
Gd3+
C
Gd3+
200 pA
50 ms
GTP-γ-S
D
3w
5w
CL
Atr
13
14
*
**
Gd3+- sensitve current
@ -60mV (pA/pF)

Figure 6. Decrease of $I_{GTP\gamma S}$ in atrophic side DFA myocytes.

Currents obtained by dialysis with 0.3 mM GTPγS in CsCl pipette solution. (A, B) Representative I/V curve detected at contralateral and atrophic side myocytes in 5w, respectively. (C) The representative I/V curves were obtained by reverse ramp pulse repolarization from 100 to -140 mV, holding potential at -10 mV. On achieving the whole cell configuration, outwardly rectifying current ($I_{GTP\gamma S}$) was spontaneously induced from negligible level (initial) to a steady-state (peak) within 3-5 min. The current was totally inhibited by 10 μM Gd^{3+}. (D) Summary of Gd^{3+}-sensitive current at -60 mV. The currents density obtained from atrophic side myocytes were smaller than the contralateral side myocytes in 3w and 5w rats. Numbers of tested cells are indicated in each bar (means ± SEM, $*P < 0.05$, $**P < 0.01$, unpaired Student's *t* test).

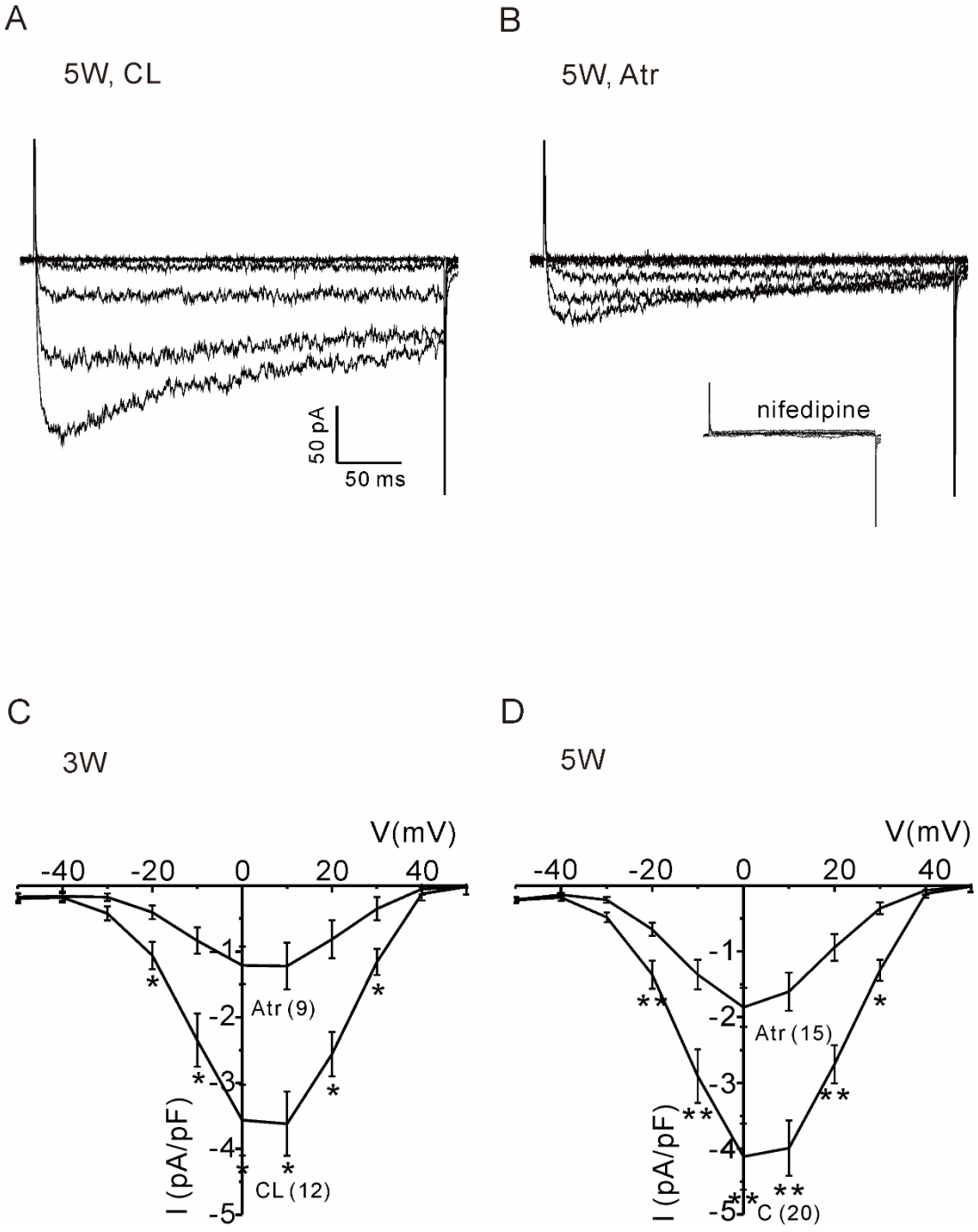
A
5W, CL
50 pA
50 ms
B
5W, Atr
nifedipine
C
3W
V(mV)
-40
-20
0
20
40
-1
-2
-3
-4
-5
Atr (9)
CL (12)
I (pA/pF)
D
5W
V(mV)
-40
-20
0
20
40
-1
-2
-3
-4
-5
Atr (15)
C (20)
I (pA/pF)

Figure 7. Decrease of L-type voltage-gated Ca^{2+} channel current ($I_{Ca,L}$) in atrophic side DFA myocytes.

(A, B) Representative current obtained by step-like depolarization from -60 to 0 mV with Cs^{+} -rich pipette solution and 10 mM of Ba^{2+} in bath solution. $I_{Ca,L}$ of myocytes isolated from contralateral side and atrophic side DFA at sedentary 5 weeks. Inset shows currents inhibited by inhibitor nifedipine. Averaged current-voltage relations (I/V curves) of the peak $I_{Ca,L}$ density (pA/pF) between Atrophic and Contralateral DFA myocytes from sedentary 3 weeks rats (C) and sedentary 5 weeks rats (D). (means ± SEM, $*P < 0.05$, $**P < 0.01$, unpaired Student's *t* test).

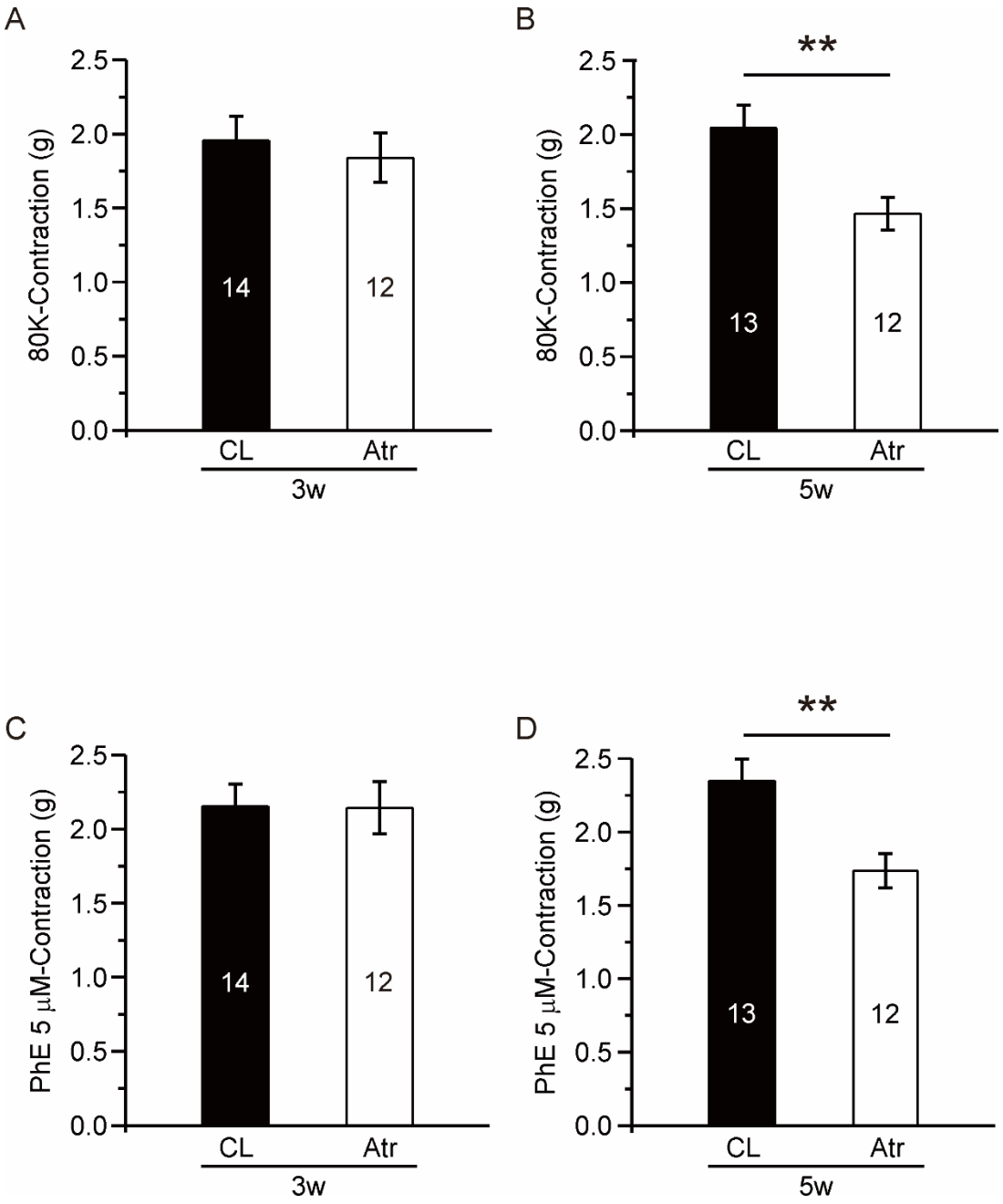
A
80K-Contraction (g)
2.5
2.0
1.5
1.0
0.5
0.0
14
12
CL
Atr
3w
B
**
80K-Contraction (g)
13
12
CL
Atr
5w
C
PhE 5 μM-Contraction (g)
14
12
CL
Atr
3w
D
**
PhE 5 μM-Contraction (g)
13
12
CL
Atr
5w

Figure 8. Reduction of vasocontractility in atrophic side DFA myocytes at sedentary 5 weeks after operation.

(A, B) Summary of contralateral and atrophic side DFA contraction induced by 80 mM KCl (80K-contraction) in sedentary 3- and 5-weeks rats. (A) There were no differences of 80K-contraction between contralateral side DFA and atrophic side DFA at 3 weeks of post-operation (3w), (B) while significantly smaller in atrophic side DFA at 5 weeks of post-operation (5w). (C, D) Summary of contralateral and atrophic side DFA contraction induced by 5 μM phenylephrine (PhE) in sedentary 3- and 5-weeks rats. PhE induced DFA contraction were reduced in atrophic side compared to the contralateral side at 5w, while no differences at 3w. (means ± SEM, $^{**}P < 0.01$, unpaired Student's *t* test).

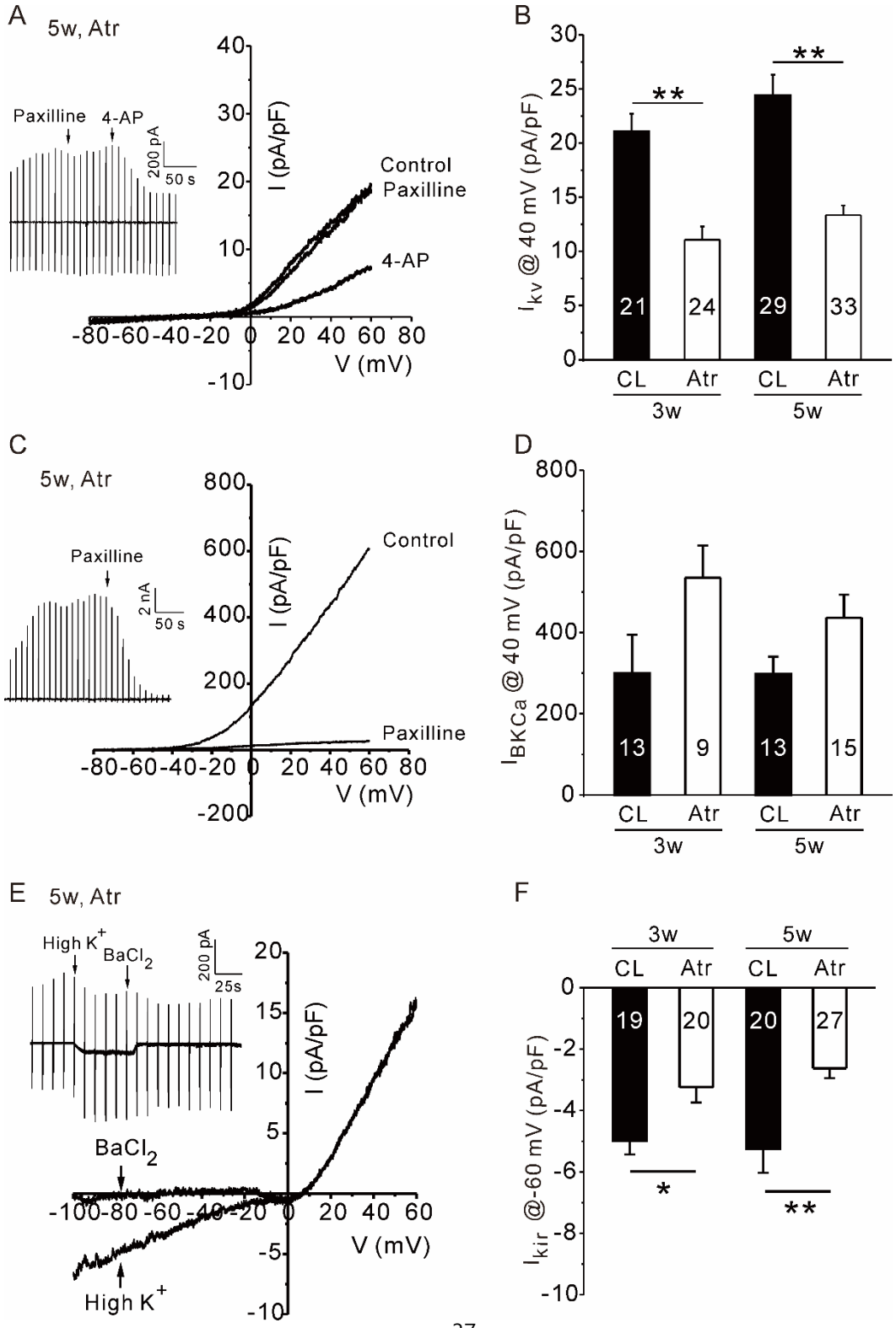
A
5w, Atr
Paxilline
4-AP
200 pA
50 s
Control
Paxilline
4-AP
I (pA/pF)
V (mV)
B
I_{kv} @ 40 mV (pA/pF)
**
**
21
24
29
33
CL
Atr
CL
Atr
3w
5w
C
5w, Atr
Paxilline
2 nA
50 s
Control
Paxilline
I (pA/pF)
V (mV)
D
I_{BKCa} @ 40 mV (pA/pF)
13
9
13
15
CL
Atr
CL
Atr
3w
5w
E
5w, Atr
High K^+
$BaCl_2$
200 pA
25s
$BaCl_2$
High K^+
I (pA/pF)
V (mV)
F
3w
5w
CL
Atr
CL
Atr
I_{kir} @-60 mV (pA/pF)
19
20
20
27
*
**

Figure 9. Amplitude of Kir and Kv channel current densities in atrophic DFA myocytes were smaller than those in contralateral DFA myocytes.

Representative membrane currents (I/V curves) in atrophic side DFA myocytes induced by ramp pulse from -80 to 60 mV (holding voltage, -80 mV) in the presence of KCl pipette solution containing 10 mM EGTA. The outward current was resistant to 1 μM paxilline, but was decreased significantly by 1 mM 4-aminopyridine (4-AP), a blocker of the voltage-gated K^+ current (I_{Kv}). (B) Summary of I_{Kv} density at 40 mV showing lower levels in Atr (n=33) monocytes than in CL myocytes (29) from 5w rats (n=9/group). (C) Representative I/V curves for atrophic side DFA myocytes induced by a ramp-like pulse from 60 to -80 mV (holding voltage, -20 mV) in the presence of 10 μM Ca^{2+}-buffered KCl pipette solution. Under these conditions, most of the outward current was abolished by paxilline, a blocker of BK_{Ca} channels. (D) Summary of I_{BKca} density at 40 mV shows no difference between Atr and CL myocytes from 5w (Atr, n=15; CL, n=13; n=3 rats/group). (E) Representative I/V curves under symmetrical KCl solutions containing 10 mM EGTA. The inward current was inhibited selectively by 100 μM BaCl, a blocker of Kir channels. (F) Summary of I_{Kir} density at -100 mV showing lower levels in Atr (n=27) than in CL (n=20) myocytes from 5w (n=6/group) rats. (means ± SEM, $*P < 0.05$, $**P < 0.01$, unpaired Student's *t* test).

Part II

Effects of endurance exercise on the skeletal artery functions in unilateral hindlimb atrophy rats.

Exercise training did not reverse the atrophy of the skeletal muscles.

In present study, the gastrocnemius and tibialis posterior muscles of hind limbs were shown atrophy after sciatic nerve denervation. The degree of muscle weight loss was similar regardless of when the rats were sacrificed and whether the rats underwent exercise training. Thus, exercise training did not improve the atrophy of the gastrocnemius and tibialis posterior muscles (Fig. 10A and B).

Paralysis decreases the DFA lumen but ET abrogates this effect.

To assess the effect of exercise training on the arterial structural changes, the atrophic and contralateral DFAs were compared 3w/ET-2w or 5w/ET-4w, by cross-sectional microscopy of Masson's trichrome stained tissue (Fig. 11A, B). As shown in Fig. 3, the total area of the atrophic side DFA was smaller than the contralateral side. By contrast, in the ET rats, the atrophic and contralateral DFAs had similar total area at both 3w/ET-2w and 5w/ET-4w (Fig. 11C). Similar observations were made with the lumen (inner) area and wall (Total-lumen) area data. Thus, first the atrophic DFAs tends to have smaller area than the contralateral DFAs at 3 postoperative weeks,

and this decrease tendency abrogated in 3w/ET-2w (Fig. 11D). Second, in the ET rats, the lumen or wall area of the atrophic and contralateral DFAs were similar regardless of when the rats were sacrificed (Fig. 11D, E).

Exercise training reverses the depressive effect of paralysis on the MR and inward cationic currents of DFAs.

To assess the effect of exercise training on MR, DFAs from the 3w/ET-2w and 5w/ET-4w were placed under stepwise increases in P_{lum}, and their contractile responses (*i.e.*, D_{in} changes) were compared with the responses of DFAs from the 3w and 5w (Fig. 12A, B). Also, the MRs of the atrophic and contralateral DFAs were compared between sedentary and exercise trained groups; 3w vs. 3w/ET-2w, and 5w vs. 5w/ET-4w (Fig. 12C, D). The contralateral DFAs all exhibited similar MRs regardless of whether they were from control or exercise training rats and whether they were harvested at 3 or 5 postoperative weeks (Fig. 12C, D, left panels). Thus, exercise training alone had no significant effect on the MR of the non-paralyzed hind limb DFAs. As described above (Fig. 4), the atrophic DFAs in the sedentary rats exhibited a loss in MR at 3 and especially 5 postoperative weeks. Interestingly, exercise training effectively abrogated these losses of MR in the atrophic DFAs at both 3 and 5 postoperative weeks (Fig. 12C, D, right panels). Consistent with the MRs, at the transmural pressure of 80 mmHg under NT solution, the D_{in} of atrophic and

contralateral DFAs were not different in both 3w/ET-2w and 5w/ET-4w (Fig. 12E). Also, the D_{in} under 0Ca-NT solution was not different between atrophic and contralateral DFA (Fig. 12F).

To assess the effect of exercise training on inwards cationic currents, the myocytes were isolated from the atrophic and contralateral DFAs of 3w/ET-2w and 5w/ET-4w. To investigate the effect of exercise training on TRPC channel currents, $I_{GTP\gamma S}$ was measured in DFA myocytes of 5w/ET-4w (Fig. 13A). The $I_{GTP\gamma S}$ densities measured in atrophic DFA myocytes were smaller than contralateral parts of 3w/ET-2w (Fig. 13B). By contrast, atrophic DFA myocytes consistently developed outwardly rectifying $I_{GTP\gamma S}$ with sizes similar to the contralateral DFA myocytes of 5w/ET-4w (Fig. 13C). Thus, exercise training abrogated the drop of $I_{GTP\gamma S}$ that was observed in the atrophic DFA myocytes from 5w. To determine the molecular nature of the $I_{GTP\gamma S}$, the DFA myocytes of sedentary or sedentary combined exercise training were subjected to RT-qPCR analysis of TRPC3, TRPC4, and TRPC6 (Fig. 13D-I). The myocytes did not differ in terms of TRPC3 and TRPC4 mRNA regardless of whether they were from the atrophic or contralateral DFA, or from the sedentary or exercise training rats in 3w and 5w (Fig. 13D, E, G and H). However, the atrophic DFA myocytes from the sedentary rats expressed significantly less TRPC6 mRNA than the contralateral DFA myocytes from 5w rats. By contrast, the myocytes from the atrophic and contralateral DFAs of 5w/ET-4w did not differ in terms of TRPC6 mRNA levels. Interestingly, both of these exercise training myocytes groups had

significantly higher TRPC6 transcript levels than the corresponding myocytes group from the sedentary rats (Fig. 13I).

The effect of exercise training on L-type Ca^{2+} channel currents of the myocytes was examined. The myocytes from atrophic DFAs in sedentary rats at 3w/ET-2w had lower $I_{Ca,L}$ densities than the myocytes from the contralateral DFAs (Fig. 14A, B). Interestingly two myocytes groups did not differ significantly in terms of the current densities of $I_{Ca,L}$ at 5w/ET-4w. Thus, the drop in $I_{Ca,L}$ that was seen in the atrophic DFA in the sedentary rats in Figure 8D was not observed in the 5w/ET-4w rats (Fig. 14C, D).

Effect of exercise training on vasocontractility.

To further assess whether the effect of exercise training on $I_{Ca,L}$ is reflected in the contractile responses, dual-wire myography was conducted for the DFAs from 3w/ET-2w and 5w/ET4w. In 3w/ET-2w, there were no statistical significant difference amplitude of 80K contraction between sedentary contralateral DFA and atrophic DFA, even though sedentary combined exercise training (Fig. 15A). By contrast, it was observed the amplitudes of 80K induced vasoconstriction of atrophic DFA were smaller than the contralateral DFA in 5w on the preceding result, and the amplitude of 80K contraction were similar in 5w/ET-4w (Fig. 15B).

In addition to the 80K contraction, effects of exercise training on phenylephrine

(PhE)-induced vasoconstriction were examined. The amplitude of 5 μM PhE induced contractions in contralateral DFA were similar to the atrophic DFA at 3 postoperative weeks (Fig. 15C), and even though in 3w/ET-2w there were no differences of contraction responses by 5 μM PhE, compared between the atrophic DFAs and the contralateral DFAs. The amplitude of PhE induced contractions in atrophic DFA were smaller than those of contralateral parts at 5 postoperative weeks, by contrast the difference were abrogated in 5w/ET-4w (Fig. 15D).

Effect of exercise training on K^+ channel currents densities in atrophic side DFA smooth muscle cells.

To assess the effect of exercise training on K^+ channel currents of the myocytes, I measured I_{Kv} densities of atrophic and contralateral myocytes in 3w/ET-2w and 5w/ET-4w rats (Fig. 18A-D). The amplitude of I_{Kv} in the atrophic side DFA myocytes were smaller than the contralateral side myocytes in 3w and the differences were abrogated in 3w/ET-2w, even the amplitude of in atrophic side DFA were tends to bigger than the contralateral side, but the statistical significant did not achieve (Fig. 16A, B). The myocytes from the atrophic DFAs from 5w had significantly lower current densities of I_{Kv} at 40 mV than the contralateral DFA myocytes (Fig. 18D). Exercise training abrogated this depressive effect of atrophy (Fig. 16C, D).

Then I measured I_{BKCa} of DFA myocyte from 3w/ET-2w and 5w/ET-4w rats (Fig. 17A-D). The atrophic side I_{BKCa} obtained from 3w even though did not achieve statistical significant, but were slightly bigger tendency compared to the contralateral side myocytes (Fig. 17B). In 3w/ET-2w rats, the tendency become smaller and in 5w/ET-4w, there no difference of amplitude of I_{BKCa} between atrophic side and contralateral side myocytes (Fig. 17D).

Finally, I measured the I_{Kir} of DFA myocytes in 3w/ET-2w and 5w/ET-4w rats to assess the effect of exercise training (Fig. 18A-D). The amplitude of I_{Kir} in atrophic myocytes obtained from 3w were significantly smaller than the contralateral side (Fig. 18B left panel). Interestingly in 3w/ET-2w rats, the amplitude of I_{Kir} atrophic side were even bigger than the contralateral side myocytes (Fig. 20B right panel). The amplitude of I_{Kir} in atrophic DFA myocytes detected in 5w were significantly smaller than the contralateral side, but the differences were abrogated in 5w/ET-4w (Fig. 18D).

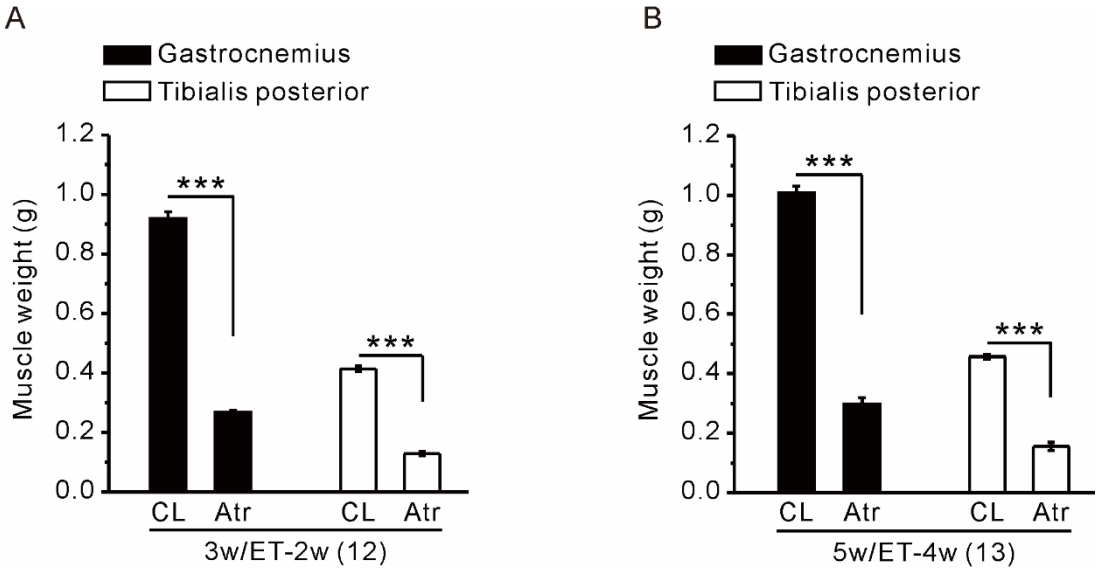

Figure 10. No recovery of atrophic muscles by exercise training.

(A) Summary of gastrocnemius and tibialis posterior muscle from sedentary 1w after combined 2 weeks of exercise training (3w/ET-2w), (B) and combined 4 weeks of exercise training (5w/ET-4w). (means ± SEM, ***$P < 0.001$, paired Student's *t* test).

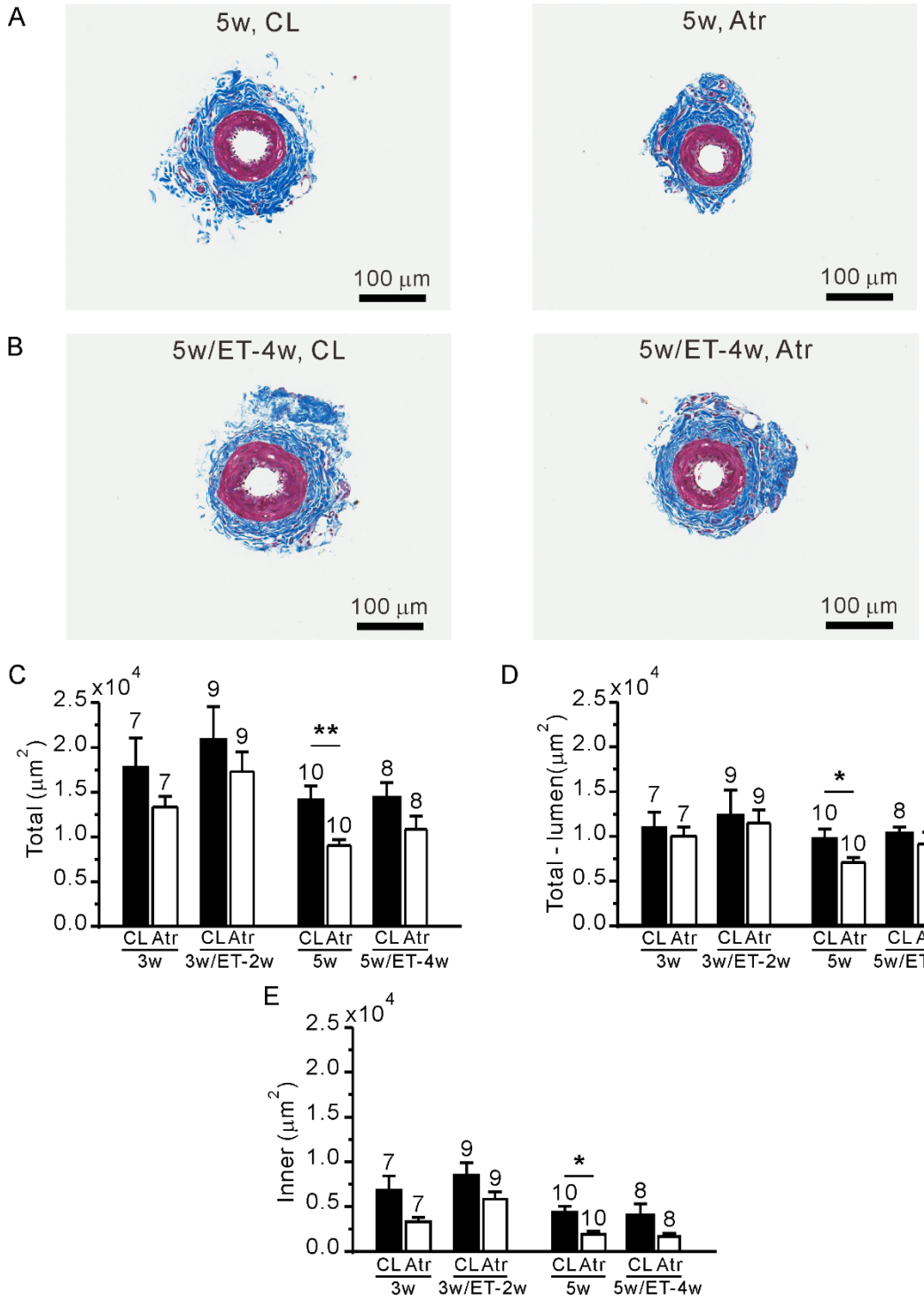
A
5w, CL
100 μm
5w, Atr
100 μm
B
5w/ET-4w, CL
100 μm
5w/ET-4w, Atr
100 μm
C
Total (μm²)
x10⁴
2.5
2.0
1.5
1.0
0.5
0.0
7
7
9
9
10
10
8
8
**
CL Atr
3w
3w/ET-2w
5w
5w/ET-4w
D
Total - lumen(μm²)
x10⁴
*
E
Inner (μm²)
x10⁴
*

Figure 11. Histological changes of DFA in exercise combined sedentary rats model.

(A, B) Representative Masson's trichrome staining image of contralateral (CL) and atrophic side DFAs from sedentary 5w and 5w/ET-4w. (C-E) Summary of total outer medial area (Total), luminal (Inner) and medial wall area (Total-lumen). Number of the samples are indicated in each bar. (means ± SEM, $*P < 0.05$, $**P < 0.01$, paired Student's *t* test).

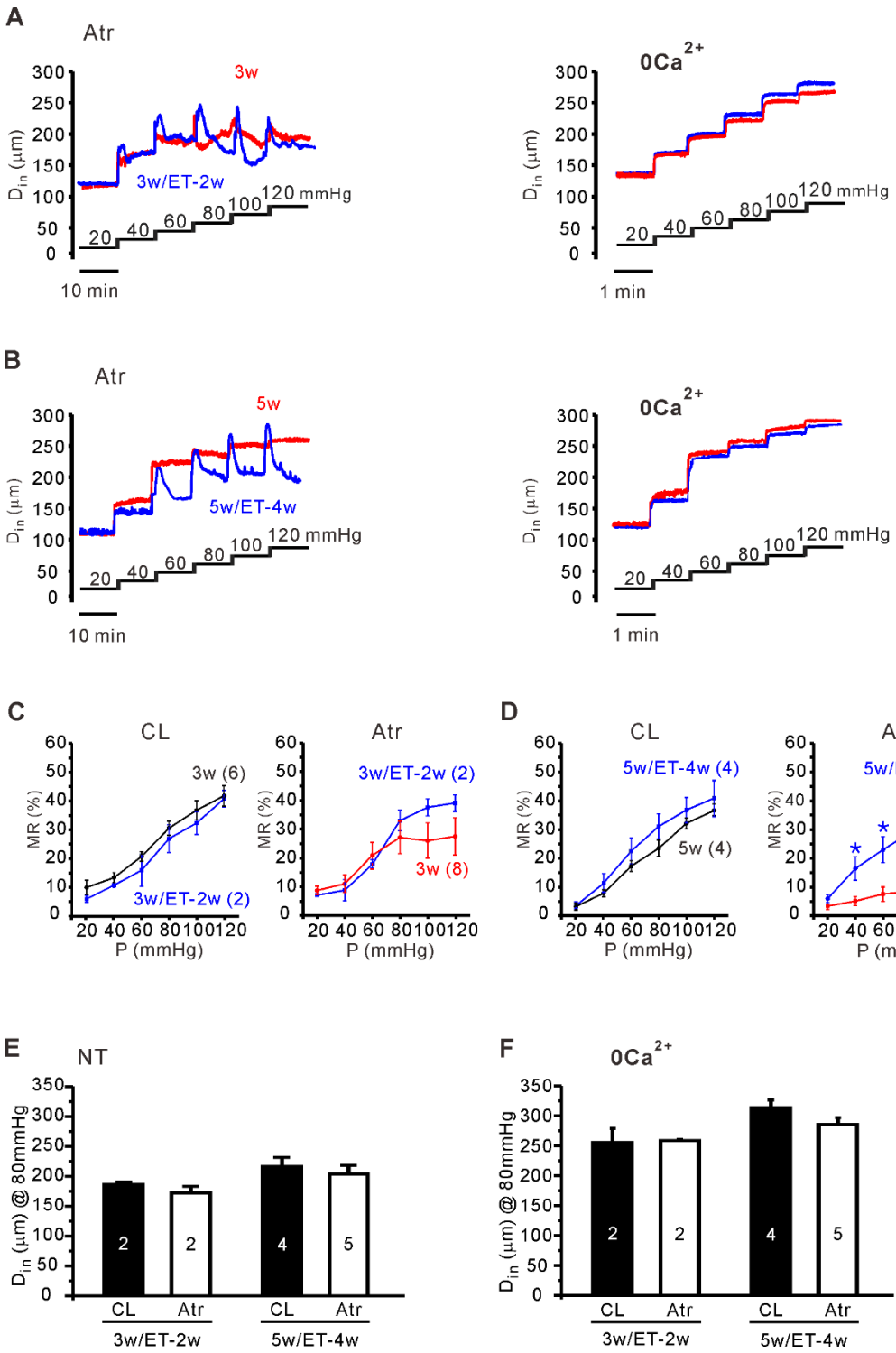
A
Atr
3w
3w/ET-2w
D_{in} (μm)
300
250
200
150
100
50
0
20 40 60 80 100 120 mmHg
10 min
$0Ca^{2+}$
1 min
B
Atr
5w
5w/ET-4w
10 min
$0Ca^{2+}$
1 min
C
CL
Atr
MR (%)
3w (6)
3w/ET-2w (2)
3w/ET-2w (2)
3w (8)
P (mmHg)
D
CL
Atr
5w/ET-4w (4)
5w (4)
5w/ET-4w (5)
5w (5)
E
NT
D_{in} (μm) @ 80mmHg
2
2
4
5
CL
Atr
3w/ET-2w
5w/ET-4w
F
$0Ca^{2+}$

Figure 12. Exercise-induced abrogation of atrophic effects on MR.

(A, B) Representative traces of D_{in} in response to stepwise increases in P_{lum} (from 20 to 120 mmHg) in atrophic side (Atr, red) DFAs from 3w (A) and 5w (B) rats. Overlaid blue traces show the D_{in} of DFAs of Atr/ET-2w (A) and Atr/ET-4w (B) rats. (C, D) Comparison of the MR of the non-atrophic (CL) and Atr DFAs of 3w (C), 5w (D), Atr/ET-2w (C), and Atr/ET-4w (D) rats. The number of tested animals is indicated in parentheses. (E, F) Summary of D_{in} at 80 mmHg of P_{lum} under NT and Ca^{2+}-free ($0Ca^{2+}$) in the DFA of 3w/ET-2w and 5w/ET-4w rats. Number of the samples are indicated in each bar. (means ± SEM, $*P < 0.05$, $**P < 0.01$, unpaired Student's *t* test).

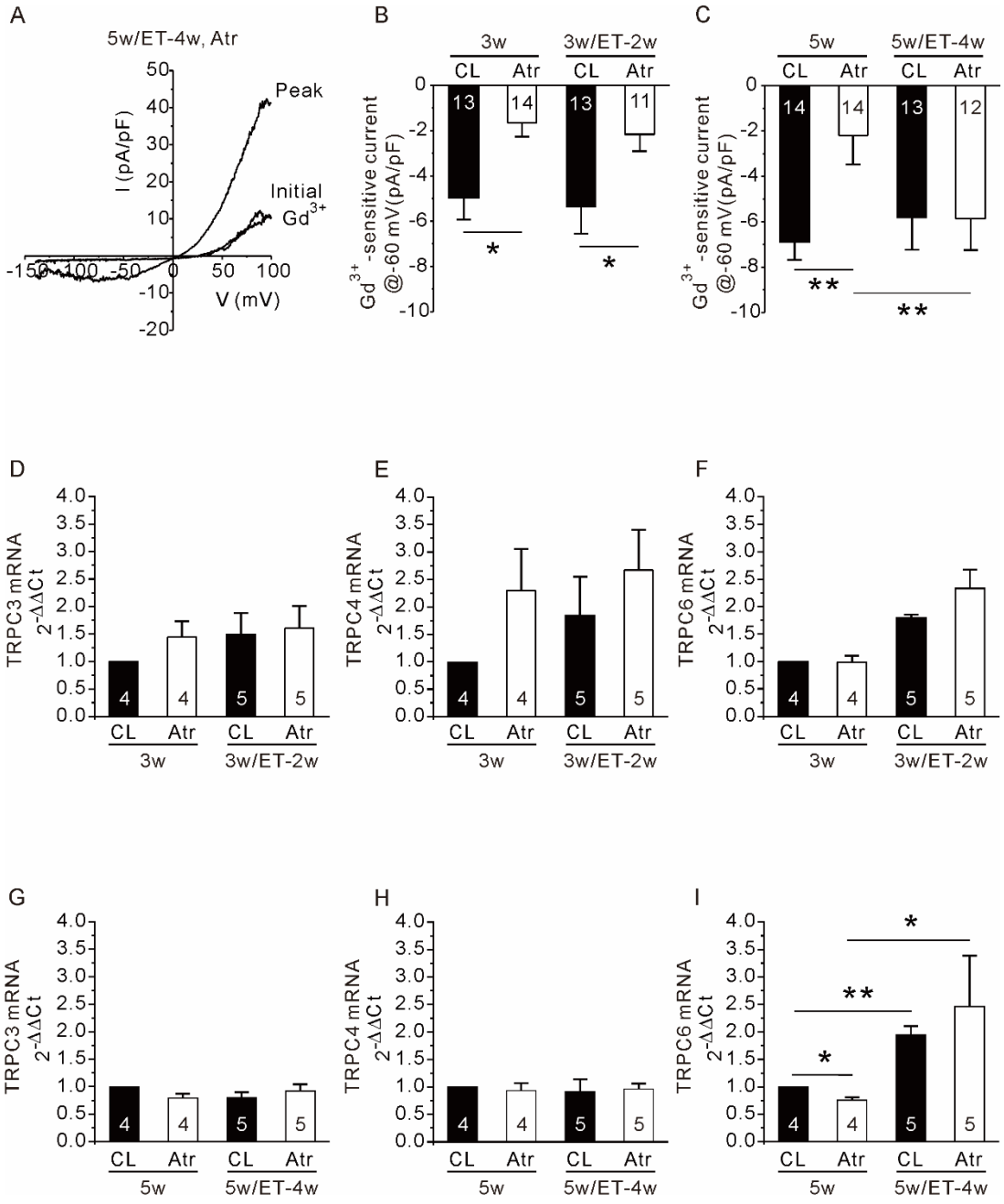
A
5w/ET-4w, Atr
Peak
Initial
Gd3+
I (pA/pF)
V (mV)
B
3w
3w/ET-2w
CL
Atr
Gd3+-sensitive current
@-60 mV(pA/pF)
C
5w
5w/ET-4w
D
TRPC3 mRNA
2-ΔΔCt
E
TRPC4 mRNA
F
TRPC6 mRNA
G
H
I

Figure 13. Effects of atrophy on $I_{GTP\gamma S}$ were abrogated in exercise trained 5w/ET-4w rats.

(A) Representative $I_{GTP\gamma S}$ results for Atr myocytes from 5w/ET-4w rats. (D) The $I_{GTP\gamma S}$ densities in Atr (n=11) were lower than CL (n=13), while the $I_{GTP\gamma S}$ densities in CL (n=13) and Atr myocytes (n=12) from 5w/ET-4w rats was similar (n=6/group). Summary of TRPC3, TRPC4, and TRPC6 mRNA levels of DFA myocytes in 3w and 3w/ET-2w (D–F) or in 5w and 5w/ET-4w (G–I). Amounts of TRPC6 transcript in Atr of 5w rats were lower than those in CL, while those in the Atr and CL of 5w/ET-4w were similar. Note that TRPC6 transcript levels in the CL and Atr were higher in 5w/ET-4w rats than in 5w rats (I). Number of the samples are indicated in each bar. (means ± SEM, $*P < 0.05$, $**P < 0.01$, unpaired Student's *t* test).

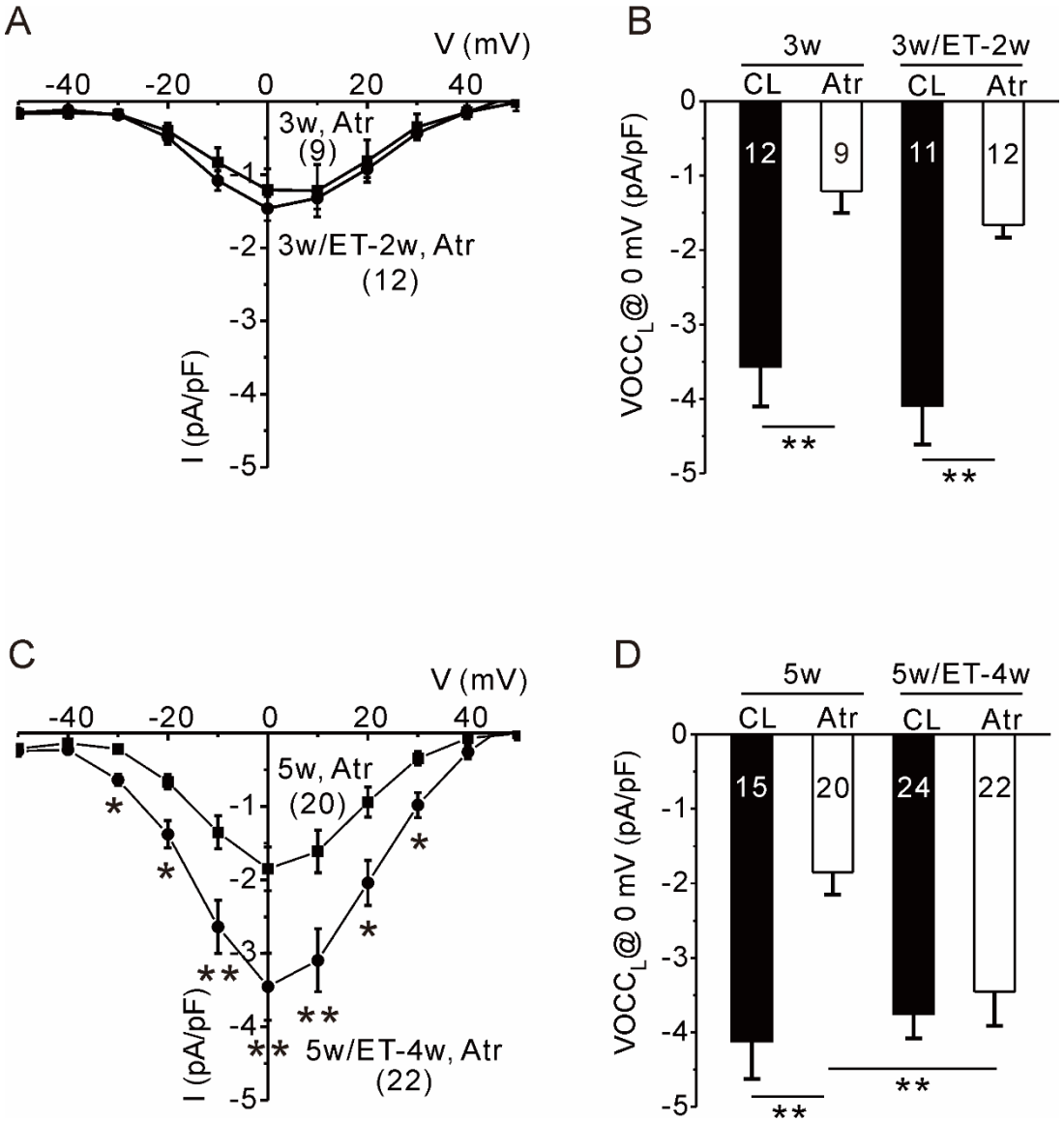
A
V (mV)
-40
-20
0
20
40
3w, Atr
(9)
3w/ET-2w, Atr
(12)
I (pA/pF)
-1
-2
-3
-4
-5
B
3w
3w/ET-2w
CL
Atr
CL
Atr
0
-1
-2
-3
-4
-5
12
9
11
12
VOCC_L@ 0 mV (pA/pF)
**
**
C
V (mV)
-40
-20
0
20
40
5w, Atr
(20)
5w/ET-4w, Atr
(22)
I (pA/pF)
-1
-2
-3
-4
-5
*
*
**
**
**
*
*
D
5w
5w/ET-4w
CL
Atr
CL
Atr
0
-1
-2
-3
-4
-5
15
20
24
22
VOCC_L@ 0 mV (pA/pF)
**
**

Figure 14. Smaller I_{CaL} densities in atrophic side DFA and abrogated in exercise trained 5w/ET-4w rats.

(A, C) Averaged current-voltage relations (I/V curves) of the peak I_{CaL} density (pA/pF) in atrophic side DFA myocytes, at 3w and 3w/ET-2w rats (A) or 5w and 5w/ET-4w rats. (B, D) Summary of the I_{CaL} at 0 mV in contralateral and atrophic side myocytes from sedentary and sedentary combine exercise trained rats. Comparisons of the I_{CaL} density obtained from atrophic side DFA myocytes in 3w/ET-2w were smaller than the contralateral side (B), by contrast the differences were abrogated in 5w/ET-4w rats (D). Number of the samples are indicated in each bar. (means ± SEM, $^{**}P < 0.01$, unpaired Student's *t* test).

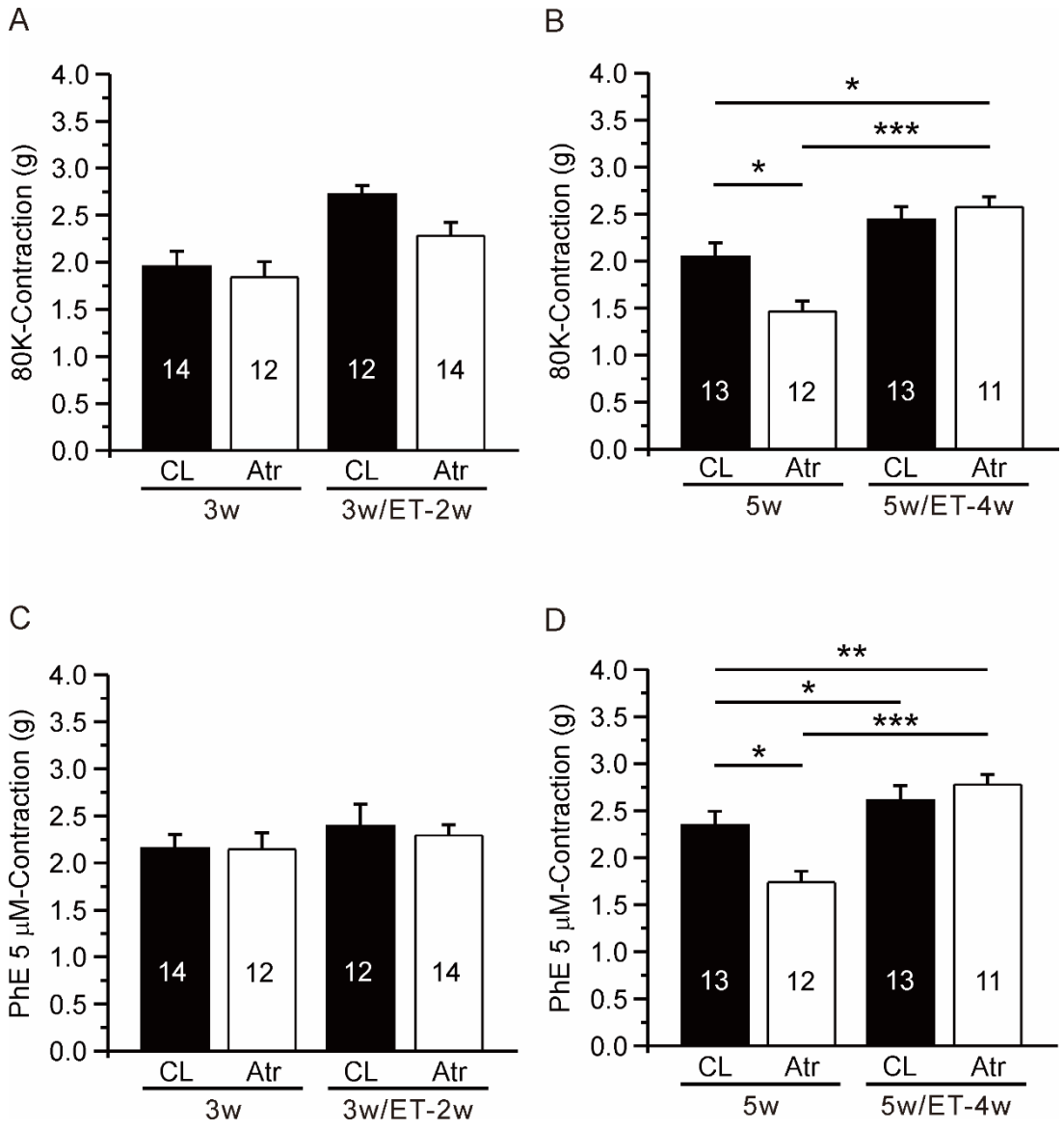
A
80K-Contraction (g)
4.0
3.5
3.0
2.5
2.0
1.5
1.0
0.5
0.0
14
12
12
14
CL
Atr
CL
Atr
3w
3w/ET-2w
B
80K-Contraction (g)
*
***
*
13
12
13
11
CL
Atr
CL
Atr
5w
5w/ET-4w
C
PhE 5 μM-Contraction (g)
14
12
12
14
CL
Atr
CL
Atr
3w
3w/ET-2w
D
PhE 5 μM-Contraction (g)
**
*
***
*
13
12
13
11
CL
Atr
CL
Atr
5w
5w/ET-4w

Figure 15. Comparisons of the ET effects on vasocontractility in DFA of sedentary and exercise trained rats.

(A, B) Summary of 80 mM KCl induced DFA contraction in sedentary and exercise combined sedentary rats from 3w, 3w/ET-2w, 5w, 5w/ET-4w group. The vasoconstriction induced by 80 mM KCl were significantly smaller in atrophic side than contralateral side DFA, and in 5w/ET-4w the difference of the contractility was abrogated (B). (C, D) Comparison of 5 μM phenylephrine (PhE) induced DFA contraction in contralateral and atrophic side from sedentary and sedentary combine exercise training rats. In 5w/ET-4w rats, PhE induced contraction were no difference between contralateral and atrophic side, while the response was smaller in atrophic side at 5w (D). Number of the samples are indicated in each bar. (means ± SEM, **P* < 0.05, ***P* < 0.01, unpaired Student's *t* test).

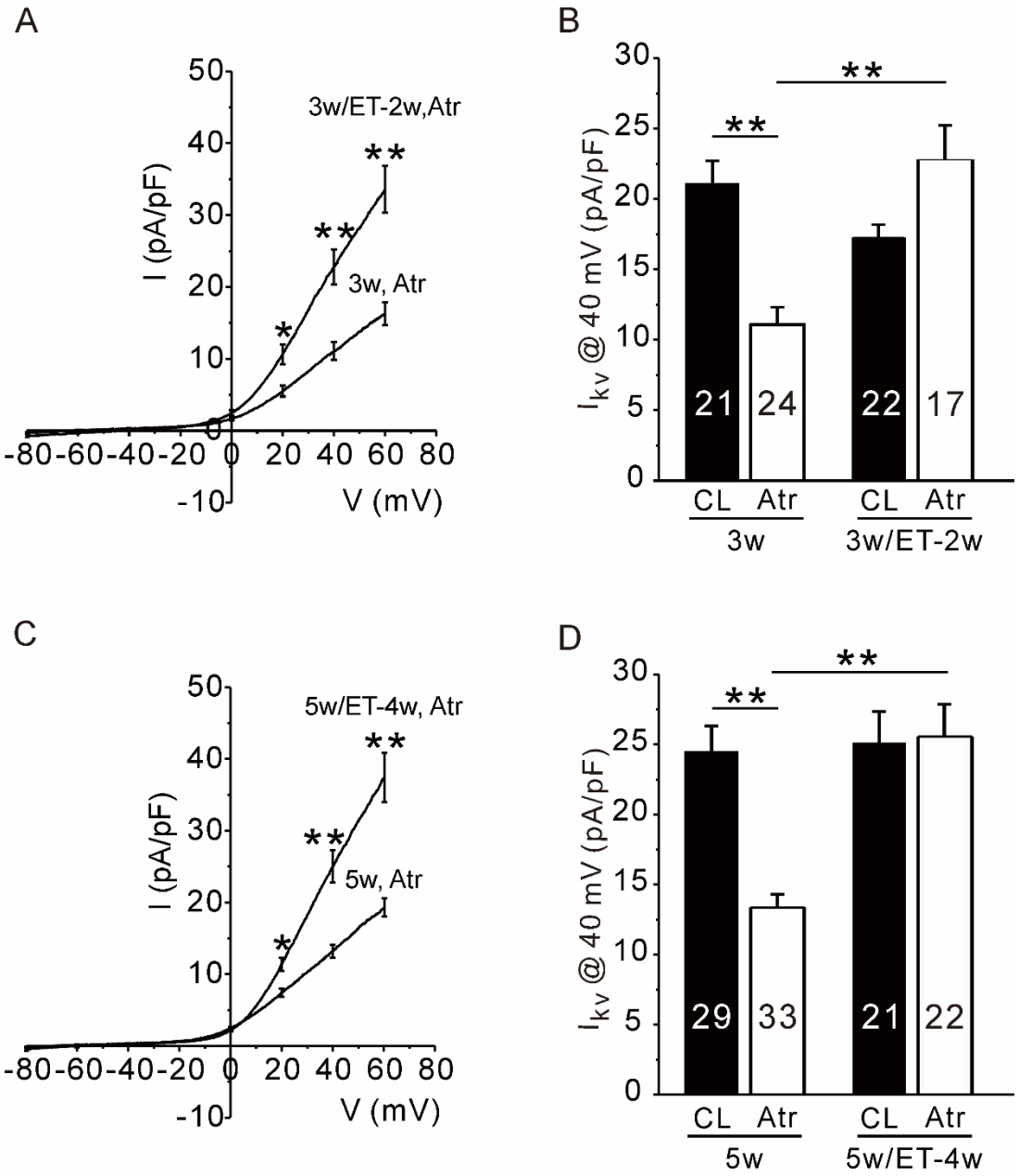
A
3w/ET-2w,Atr
3w, Atr
I (pA/pF)
V (mV)
B
I_{kv} @ 40 mV (pA/pF)
21
24
22
17
CL
Atr
3w
3w/ET-2w
C
5w/ET-4w, Atr
5w, Atr
D
29
33
21
22
5w
5w/ET-4w

Figure 16. Smaller I_{Kv} in atrophic side DFA and recovery by exercise training.

Using KCl pipette solution containing 10 mM EGTA and NT bath solution, I/V curves were obtained by ramp pulse from -80 to 60 mV (holding voltage, -60 mV), and normalized to the membrane capacitance (pA/pF). Numbers of tested cells are indicated in each panel. (A, C) Averaged I/V curves of I_{Kv} in atrophic side DFA myocytes obtained from 3w, 3w/ET-2w, 5w and 5w/ET-4w. (B, D) Summary of current density at 40 mV. Comparisons of I_{Kv} between atrophic side and contralateral side shown smaller densities in atrophic side at 3w and 5w, by contrast the difference of the density was abrogated in 3w/ET-2w and 5w/ET-4w (B, D). Number of the samples are indicated in each bar. (means ± SEM, $*P < 0.05$, $**P < 0.01$, unpaired Student's *t* test).

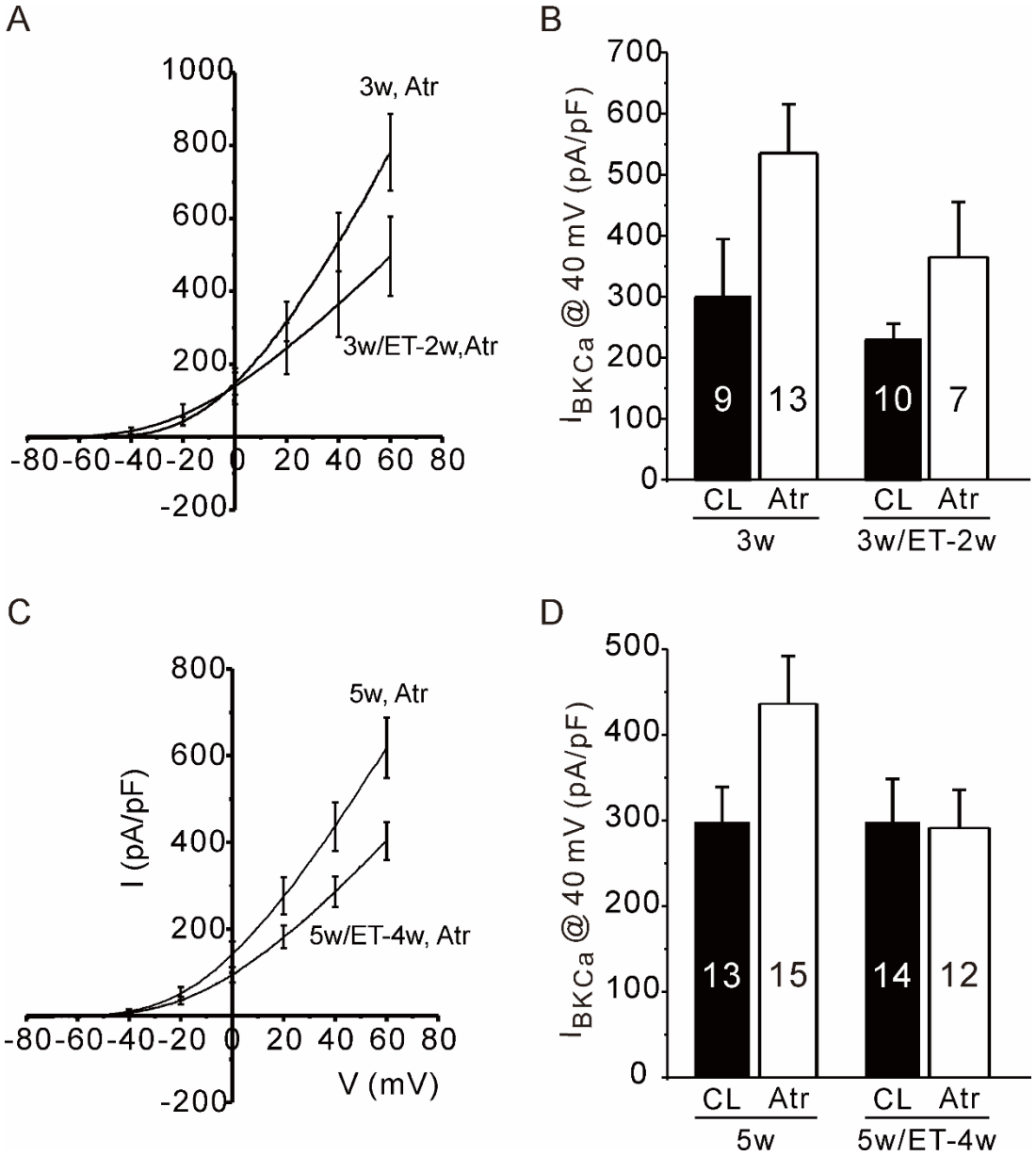
A
1000
800
600
400
200
-200
-80 -60 -40 -20 0 20 40 60 80
3w, Atr
3w/ET-2w,Atr
B
700
600
500
400
300
200
100
0
I_{BKCa} @ 40 mV (pA/pF)
9
13
10
7
CL Atr
CL Atr
3w
3w/ET-2w
C
800
600
400
200
-200
I (pA/pF)
-80 -60 -40 -20 0 20 40 60 80
V (mV)
5w, Atr
5w/ET-4w, Atr
D
500
400
300
200
100
0
I_{BKCa} @ 40 mV (pA/pF)
13
15
14
12
CL Atr
CL Atr
5w
5w/ET-4w

Figure 17. Comparison of I_{BKCa} in DFA myocytes between atrophic and contralateral side.

Using KCl pipette solution with 10 μM Ca^{2+} activity and NT bath solution, I/V curve were obtained by reverse ramp pulse from -80 to 60 mV (holding voltage, -20 mV), and normalized to the membrane capacitance (pA/pF). Number of tested cells are indicated in each panel. (A, C) Averaged I/V curves of I_{BKCa} in atrophic side from sedentary and sedentary combine exercise trained rats. (B, D) Summary of the currents density at 40 mV in 3w, 3w/ET-2w, 5w and 5w/ET-4w. Number of the samples are indicated in each bar.

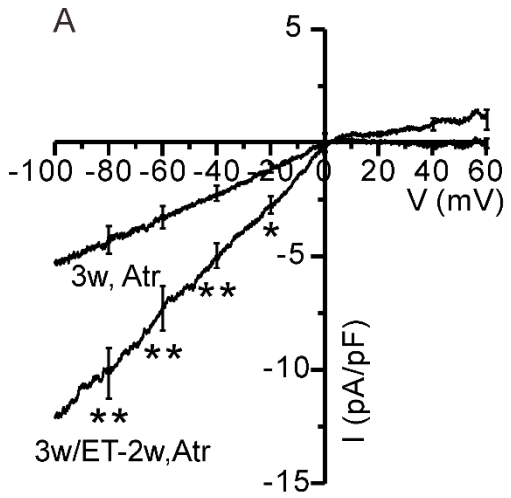
A
5
-100 -80 -60 -40 -20 0 20 40 60
V (mV)
-5
-10
-15
I (pA/pF)
3w, Atr
3w/ET-2w,Atr
*
**
**
**

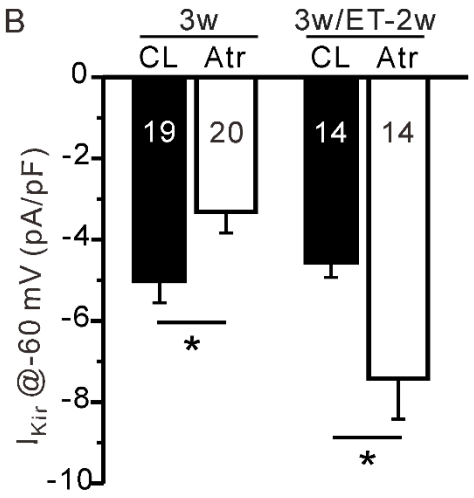
B
3w
3w/ET-2w
CL
Atr
CL
Atr
0
-2
-4
-6
-8
-10
I_{Kir} @-60 mV (pA/pF)
19
20
14
14
*
*

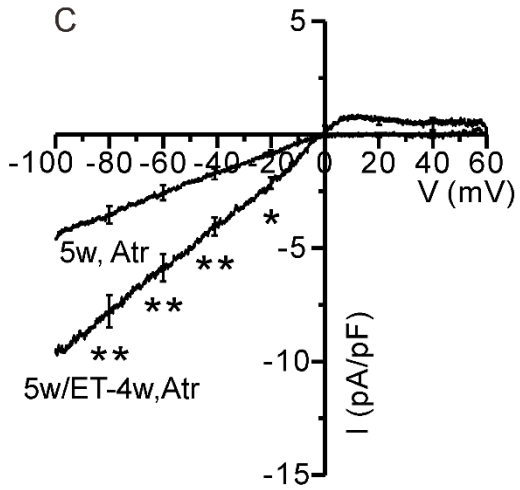
C
5
-100 -80 -60 -40 -20 0 20 40 60
V (mV)
-5
-10
-15
I (pA/pF)
5w, Atr
5w/ET-4w,Atr
*
**
**
**

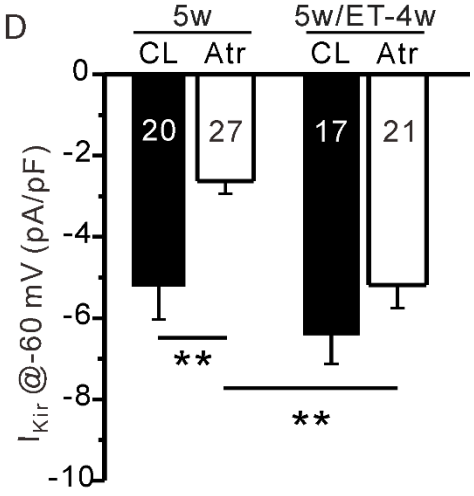
D
5w
5w/ET-4w
CL
Atr
CL
Atr
0
-2
-4
-6
-8
-10
I_{Kir} @-60 mV (pA/pF)
20
27
17
21
**
**

Figure 18. Effects of ET on I_{Kir} in atrophic DFA and contralateral DFA myocytes.

Using symmetrical KCl solution in pipette and bath, I/V curves were obtained by ramp pulse hyperpolarization from 60 to -100 mV, and normalized to the membrane capacitance (pA/pF). Total inhibition of the inwardly rectifying current by 100 mM Ba^{2+} was confirmed in each cell, and the Ba^{2+}-sensitive current (I_{Kir}) was analyzed. (A, C) Comparisons averaged I/V curves of I_{Kir} in atrophic side myocytes between sedentary and sedentary combine exercise trained rats. (B, D) Summary of the currents density at -60 mV in 3w, 3w/ET-2w, 5w and 5w/ET-4w. Number of the samples are indicated in each bar.

DISCUSSION

Here, I used unilateral sciatic denervation model rats to investigate the MRs and ionic currents of arteries feeding the lower hindlimb muscles. The atrophic side DFAs of 5w rats exhibited poor MRs and depressed ionic currents in myocytes. Intriguingly, exercise training of 5w/ET-4w rats prevented the loss of functional parameters associated with paralysis. Although a few previous studies on hindlimb-unloaded or spaceflight-exposed animals show that atrophy diminishes both the MR and agonist-induced contractions in skeletal arterioles (Delp, 1999; Stabley et al., 2012), the cellular mechanisms underlying these alterations were not directly investigated. My results showed clear evidence that loss and recovery of MR along with TRPC6-like current and mRNA levels of the skeletal arteries in paralyzed hindlimb. The vasocontractility in atrophic side DFA myocytes.

In comparison with microgravity conditions or hindlimb-unloaded animal models, our model is technically simple and therefore suitable for studies that require a large number of tissue samples or cells. Furthermore, the contralateral limbs can serve as an internal sham surgery control. Unilateral sciatic denervation did not seem to affect the feeding behavior of animals because their body weight was no different from that of age-matched control rats. Moreover, the unilateral sciatic-denervated rats could still exercise on a rodent treadmill, which enabled us to investigate the effects of endurance exercise training on the affected vessels.

Previous studies, especially *in vivo* studies of patients with motor nerve or spinal cord injury, show that paralysis is associated with decreased conduit artery diameter, increased peripheral resistance, and decreased maximum blood flow (Olive et al., 2003; Langille & O'Donnell, 1986; West et al., 2013). Our histology results showing that atrophic DFA in 5w rats had a smaller cross-sectional area than the contralateral DFA (Fig. 3C-E, and Fig. 4C-E) seem to be consistent with previous studies. However, we found that the passive diameter, i.e., D_{in} under Ca^{2+}-free NT, of pressurized arteries in 5w rats was not significantly different between atrophic and contralateral DFAs (Fig. 5G). I cannot explain the different results between fixed tissue samples and fresh arteries under physiological pressure. Although the DFAs used in this study were feeding arteries with relatively smaller diameter rather than intramuscular arterioles, the rat DFAs consistently showed MRs under a wide range of pressures, as demonstrated in our previous study (Suh et al., 2017). However, the similar passive D_{in} indicates that reduced MR in atrophic DFAs was not due to decreased D_{in} at baseline, *i.e.*, a limitation to further contraction of arteries.

Here, I confirmed that unilateral sciatic denervation rapidly induced atrophy of the affected hindlimb, but not that of the other intact limbs. Paralyzed skeletal muscles undergo rapid atrophy with increased fibrous connective tissue and fat (Carlson, 2014). Despite an increase in fibro-adipose perivascular tissue under the surgical microscopic view (Fig. 1D), I did not perform a quantitative analysis. Early atrophy was followed by disappearance of MR and drops in the depolarizing inward currents

($I_{Ca,L}$ and $I_{GTP\gamma S}$) and the I_{Kv} and I_{Kir} of the skeletal artery smooth muscle cells. Notably, endurance exercise training prevented decay of the MR and the $I_{Ca,L}$, $I_{GTP\gamma S}$, I_{Kv}, and I_{Kir} currents in the DFA of the atrophic limb.

Considering that paralysis and atrophy preceded functional decay of the DFAs, it is likely that putative alterations in regional blood flow might induce the functional changes that I observed. Alternatively, it is possible that these functional changes were caused by changes in the perivascular tissues; the loss of muscle and increased amount of fibro-adipose tissue surrounding the DFA may have altered unidentified paracrine factors. However, the fact that exercise training blocked the deleterious effects of paralysis on DFA function, but did not prevent muscle atrophy, suggests that the systemic or hemodynamic influences were more likely to be factors that promote long-term functional changes.

Potential changes in hemodynamic stimuli (*e.g.*, shear stress) would affect the endothelium of corresponding vessels directly. Considering the importance of endothelial cells and their responsiveness to mechanical stress, it is possible that functional changes in the smooth muscles of atrophic DFAs may be driven by the endothelium. In addition, it is also possible that putative mechanical stimuli to the medial layer (*e.g.*, pulsatile changes in wall tension during exercise) may have driven the observed changes in smooth muscle function in the present study. Despite the intriguing functional changes in skeletal arterial smooth muscles, the mechanistic

explanation is still limited, and further studies are warranted, including study of the changes in endothelial ion channels and Ca^{2+} signaling.

Changes in $I_{Ca,L}$ and $I_{GTP\gamma S}$

I found that both the $I_{Ca,L}$ and $I_{GTP\gamma S}$ of atrophic DFA myocytes decreased, and that these effects were abrogated by exercise training. Ca^{2+} influx *via* L-type Ca^{2+} channels are critical for depolarization-induced contraction, as demonstrated in Ca_V 1.2-knockout mice (Moosmang et al., 2003). Therefore, the common direction of the changes in $I_{Ca,L}$ and $I_{GTP\gamma S}$ in our study suggests that long-term electrophysiological responses may underlie the observed changes in MR. A previous study also showed that exercise training facilitates $I_{Ca,L}$ in swine coronary arteries (Bowles, 2001). However, voltage-dependent Ca^{2+} channels are generally regarded as the effector component of the MR in pressurized arteries, whereas TRPC channels are thought to serve as a sensing component (Sharif-Naeini et al., 2010; Tykocki et al., 2017).

It was found that transcription of TRPC6 in atrophic DFA myocytes was downregulated, and that exercise training abrogated this effect (Fig. 15D-I). Thus, it is highly likely that TRPC6 drives the paralysis- and exercise training-associated changes in the $I_{GTP\gamma S}$ in arterial myocytes. The weakly outward rectifying I/V curve of $I_{GTP\gamma S}$ was also consistent with this electrophysiological property of TRPC6 (Sharif-Naeini et al., 2010).

The importance of TRPC6 as a mechanosensitive ion channel in vascular smooth muscle was suggested by an early study (Spassova et al., 2006). However, rather than inherent mechanosensitivity (*i.e.*, direction activation of TRPC6), an interplay between Gq/11 protein-coupled receptors and TRPC channels, followed by membrane stretch, has been suggested as an acceptable mechanism for myogenic vasoconstriction (Inoue et al., 2009; Mederos et al., 2008). Although a change of the mechanosensitivity could not be excluded, the increased activation of TRPC6-like currents by dialyzing against GTPγS and increased TRPC6 mRNA suggest the upregulation of final signaling pathway, i.e. TRPC6 channel, rather than just surrogate stimulation of the channel.

The present results show that both the MR and $I_{GTP\gamma S}$ recovered in exercise-trained rats, strongly suggesting that TRPC plays an important role in skeletal arterial MR. Consequently, it may be a long-term regulatory target of atrophic disuse in addition to exercise training. The concomitant changes in $I_{Ca,L}$ could be reflected, at least in part, by contractile responses to membrane depolarization of arteries, as demonstrated by changes in high-K contraction (Fig. 9B and Fig. 17B). Despite the intriguing changes in $I_{Ca,L}$ and $I_{GTP\gamma S}$, however, no direct mechanical stimuli was applied to arterial myocytes. Considering that the electrophysiological mechanism underlying MR requires mechanosensitive ion channels, further investigation of ionic currents augmented by membrane stretch conditions is necessary.

Changes in K^+ currents

K^+ channels are electrically negative feedback regulators in vascular smooth muscle cells; Kv and BK_{Ca} are activated mainly by membrane depolarization and increases in $[Ca^{2+}]_i$, respectively. In addition, the Kir2.x channel contributes to the negative resting membrane potential and K^+-vasodilation mechanisms in resistance arteries (Tykocki et al., 2017). In this respect, the lower density of I_{Kv} and I_{Kir} in the DFA myocytes from atrophic limbs may themselves imply putative pro-contractile changes. Nevertheless, the decreases in $I_{GTP\gamma S}$ and $I_{Ca,L}$ might have counter balanced the decreases in I_{Kv} and I_{Kir} in the atrophic DFA.

Although the result did not achieve statistical significance, atrophic DFA myocytes tended to exhibit higher I_{BKCa} (Fig. 10D). This response may also oppose decreases in I_{Kv} and I_{Kir}. Interestingly, previous studies on I_{BKCa} show that (as opposed to other K^+ channel currents) it exhibits increased current density under pathological conditions such as hypertension, and that exercise training reverses this (Li et al., 2013; Shi et al., 2016; Zhang et al., 2017). Since the contribution of BK_{Ca} to setting the basal contractility and MR are different between artery types, further investigations might reveal actual increases in I_{BKCa} in the vessels perfusing disused tissue (Suh et al., 2017).

Summary and physiological implications

Taken together, the results presented herein demonstrate that exercise training abrogates the decay of MR along with $I_{Ca,L}$, $I_{GTP\gamma S}$ (TRPC6), I_{Kv}, and I_{Kir} in atrophic DFA smooth muscle. Although the wide-ranging effects of paralyzed atrophy and

exercise on various ionic current densities were quite impressive, this study could not elucidate the mechanisms underlying the changes in the MR and ionic currents. In other words, the mechanisms which directly associate with the electrophysiological changes should be identified further in *in vivo* conditions. Nevertheless, treadmill-running performed by unilateral hindlimb-paralyzed rats may be a useful experimental model for investigating how rehabilitation exercise affects vascular function, particularly the MR and its associated ionic currents, in paralyzed limbs. A probable increase in hemodynamic stimuli in skeletal artery smooth muscle may play an important role in maintaining MR and ionic currents in skeletal artery smooth muscle. Since spinal cord injury affects not only the motor but also sensory and autonomic nerves, other factors also participate in the positive effects of rehabilitation exercise protocols on paralyzed patients. In this respect, the unilateral hindlimb atrophy model may be useful for addressing more specific questions related to vascular pathophysiology due to motor nerve paralysis or disuse atrophy.

REFERENCE

Abramowitz J, Birnbaumer L. Physiology and pathophysiology of canonical transient receptor potential channels. FASEB J 23: 297-328, 2009.

Baek EB, Jin C, Park SJ, Park KS, Yoo HY, Jeon JH, Earm YE, Kim SJ. Differential recruitment of mechanisms for myogenic responses according to luminal pressure and arterial types. Pflugers Arch 460:19-29, 2010.

Bowles DK. Gender influences coronary L-type Ca^{2+} current and adaptation to exercise training in miniature swine. J Appl Physiol (1985) 91: 2503-2510, 2001.

Calbet JA, Lundby C. Skeletal muscle vasodilatation during maximal exercise in health and disease. J Physiol 590:6285-6296, 2012.

Carlson BM. The biology of long-term denervated skeletal muscle. Eur J Transl Myol 24: 3293, 2014.

Crecelius AR, Richards JC, Luckasen GJ, Larson DG, Dinenno FA. Reactive hyperemia occurs via activation of inwardly rectifying potassium channels and Na^{+}/K^{+}-ATPase in humans. Circ Res 113: 1023-1032, 2013.

Delp MD. Myogenic and vasoconstrictor responsiveness of skeletal muscle arterioles is diminished by hindlimb unloading. J Appl Physiol (1985) 86: 1178-1184, 1999.

Gonzales AL, Yang Y, Sullivan MN, Sanders L, Dabertrand F, Hill-Eubanks DC, Nelson MT, Earley S. A PLCγ1-Dependent, Force-Sensitive Signaling Network in the Myogenic Constriction of Cerebral Arteries. Sci Signal 7: ra49, 2014.

Green DJ, Spence A, Rowley N, Thijssen DH, Naylor LH. Vascular adaptation in

athletes: is there an 'athlete's artery'? Exp Physiol 97: 295-304, 2012.

Green DJ, Hopman MT, Padilla J, Laughlin MH, Thijssen DH. Vascular adaptation to exercise in humans: Role of hemodynamic stimuli. Physiol Rev 97: 495-528, 2017.

Harder, D. R. Pressure-dependent membrane depolarization in cat middle cerebral artery. *Circ Res* 55: 197-202, 1984.

Heaps CL, Bowles DK. Nonuniform changes in arteriolar myogenic tone within skeletal muscle following hindlimb unweighting. J Appl Physiol (1985) 92: 1145-1151, 2002.

Hill MA, Meininger GA. Arteriolar vascular smooth muscle cells: mechanotransducers in a complex environment. Int J Biochem Cell Biol 44: 1505-1510, 2012.

Hill-Eubanks DC, Gonzales AL, Sonkusare SK, Nelson MT. Vascular TRP channels: performing under pressure and going with the flow. Physiology (Bethesda) 29: 343-360, 2014.

Hopman MT, van Asten WN, Oeseburg B. Changes in blood flow in the common femoral artery related to inactivity and muscle atrophy in individuals with longstanding paraplegia. Adv Exp Med Biol 388: 379-383, 1996.

Hopman MT, Groothuis JT, Flendrie M, Gerrits KHL, Houtman S. Increased vascular resistance in paralyzed legs after spinal cord injury is reversible by training. J Appl Physiol 93: 1966-1972, 2002.

Inoue R, Jensen LJ, Jian Z, Shi J, Hai L, Lurie AI, Henriksen FH, Salomonsson M,

Morita H, Kawarabayashi Y, Mori M, Mori Y, Ito Y. Synergistic activation of vascular TRPC6 channel by receptor and mechanical stimulation via phospholipase C/diacylglycerol and phospholipase A2/omega-hydroxylase/20-HETE pathways. Circ Res 104: 1399-1409, 2009.

Jin CZ, Kim HS, Seo EY, Shin DH, Park KS, Chun YS, Zhang YH, Kim SJ. Exercise training increases inwardly rectifying K^+ current and augments K^+-mediated vasodilatation in deep femoral artery of rats. Cardiovasc Res 91: 142-150, 2011.

Juel C, Olsen S, Rentsch RL, Gonza´lez-Alonso J, Rosenmeier JB. K^+ as a vasodilator in resting human muscle: implications for exercise hyperaemia. Acta Physiol (Oxf) 190: 311-318, 2007.

Thijssen DH, Maiorana AJ, O'Driscoll G, Cable NT, Hopman MT, Green DJ. Impact of inactivity and exercise on the vasculature in humans. Eur J Appl Physiol 108: 845-875, 2010.

Nash MS, Montalvo BM, Applegate B. Lower extremity blood flow and responses to occlusion ischemia differ in exercise-trained and sedentary tetraplegic persons. Arch Phys Med Rehabil 77: 1260-1265, 1996.

Langille BL, O'Donnell F. Reductions in arterial diameter produced by chronic decreases in blood flow are endothelium-dependent. Science 231: 405-407,1986.

West CR, Alyahya A, Laher I, Krassioukov A. Peripheral vascular function in spinal cord injury: a systematic review. Spinal Cord 51: 10-19, 2013.

Thijssen DH, De Groot PC, van den Bogerd A, Veltmeijer M, Cable NT, Green

DJ, Hopman MT. Time course of arterial remodeling in diameter and wall thickness above and below the lesion after a spinal cord injury. Eur JAppl Physiol 112: 4103-4109, 2012.

Kotecha N, Hill MA. Myogenic contraction in rat skeletal muscle arterioles: smooth muscle membrane potential and Ca^{2+} signaling. Am J Physiol Heart Circ Physiol 289: 1326-1334, 2005.

Li N, Shi Y, Shi L, Liu Y, Zhang Y. Effects of aerobic exercise training on large-conductance Ca^{2+}-activated K^+ channels in rat cerebral artery smooth muscle cells. Eur J Appl Physiol 113: 2553-2563, 2013.

Mederos y Schnitzler M, Storch U, Meibers S, Nurwakagari P, Breit A, Essin K, Gollasch M, Gudermann T. Gq-coupled receptors as mechanosensors mediating myogenic vasoconstriction. EMBO J 27: 3092–3103, 2008.

Moosmang S, Schulla V, Welling A, Feil R, Feil S, Wegener JW, Hofmann F, Klugbauer N. Dominant role of smooth muscle L-type calcium channel Cav1.2 for blood pressure regulation. EMBO J 22: 6027-6034, 2003.

Olive JL, Dudley GA, McCully KK. Vascular remodeling after spinal cord injury. Med Sci Sports Exerc 35: 901-907, 2003.

Saltin B. Exercise hyperaemia: magnitude and aspects on regulation in humans. J Physiol 583: 819-823, 2007.

Seo EY, Kim HJ, Zhao ZH, Jang JH, Jin CZ, Yoo HY, Zhang YH, Kim SJ. Low K^+ current in arterial myocytes with impaired K^+-vasodilation and its recovery by

exercise in hypertensive rats. Pflugers Arch 466: 2101-2111, 2014.

Sharif-Naeini R, Folgering JH, Bichet D, Duprat F, Delmas P, Patel A, Honoré E. Sensing pressure in the cardiovascular system: Gq-coupled mechanoreceptors and TRP channels. J Mol Cell Cardiol 48: 83-89, 2010.

Shi L, Zhang Y, Liu Y, Gu B, Cao R, Chen Y, Zhao T. Exercise prevents upregulation of RyRs-BKCa coupling in cerebral arterial smooth muscle cells from spontaneously hypertensive rats. Arterioscler Thromb Vasc Biol 36: 1607-1617, 2016.

Spassova MA, Hewavitharana T, Xu W, Soboloff J, Gill DL. A common mechanism underlies stretch activation and receptor activation of TRPC6 channels. Proc. Natl Acad. Sci. USA 103: 16586–16591, 2006.

Stabley JN, Dominguez JM 2nd, Dominguez CE, Mora Solis FR, Ahlgren J, Behnke BJ, Muller-Delp JM, Delp MD. Spaceflight reduces vasoconstrictor responsiveness of skeletal muscle resistance arteries in mice. J Appl Physiol (1985) 113: 1439-1445, 2012.

Suh EY, Yin MZ, Lin H, Zhang YH, Yoo HY, Kim SJ. Maxi-K channel (BK_{Ca}) activity veils the myogenic tone of mesenteric artery in rats. Physiol Rep 5(14), pii: e13330, 2017.

Tykocki NR, Boerman EM, Jackson WF. Smooth Muscle Ion Channels and Regulation of Vascular Tone in Resistance Arteries and Arterioles. Compr Physiol 7: 485-581, 2017.

Zhang Y, Chen Y, Zhang L, Lu N, Shi L. Aerobic exercise of low to moderate intensity corrects unequal changes in BK_{Ca} subunit expression in the mesenteric arteries of spontaneously hypertensive rats. Physiol Res 66: 219-233, 2017.

국문 초록

운동신경 손상은 해당 근육의 마비와 근 위축(atrophy)을 일으킨다. 근 위축 시 골격근 동맥의 혈류 감소 및 해당 골격근 동맥의 구조적 변화가 보고된 바 있지만, 골격근 동맥평활근의 기능 변화에 대한 연구는 부족하다. 본 연구에서는 좌골신경의 절단으로 일측성 하지마비와 골격근위축을 유발시킨 백서에서 골격근 동맥의 근원성수축과 평활근세포의 이온통로 변화를 관찰하였다. 또한, 일측성 하지마비로 인한 근 위축과 동맥기능 변화가 지구력 운동으로 개선되는지 알아보기 위해 한쪽 다리 좌골신경을 손상시킨 후 2주 또는 4주간 설치류 트레드밀을 사용한 운동을 진행하였다.

좌골신경 손상 후 골격근 위축은 1주차부터 관찰되었으나, 골격근동맥 근원성수축의 소실은 손상 5주 후 확인할 수 있었다. 3주와 5주차 좌골신경 손상모델의 마비된 다리 골격근동맥 평활근세포는 L-형 칼슘통로 ($VOCC_L$) 전류가 대조군(비마비 하지 동맥평활근세포)에 비해 감소하였다. 이에 상응하는 현상으로, 고농도 포타슘용액으로 유발되는 탈분극성 수축 감소 또한 골격근동맥에서 확인되었다. 근원성수축반응에 중요하다고 알려진 TRPC 전류가 감소되었으며, TRPC6 발현량 감소를 real-time PCR 분석법으로 확인하였다. 전압 의존성 포타슘통로 (Kv)

전류와 내향정류성 포타슘 통로 (Kir) 전류가 반대쪽 신경손상을 받지 않은 다리에 비해 감소되었다.

4주간 운동훈련을 병행한 좌골신경손상 백서는 마비측 하지의 골격근위축은 그대로였지만, 골격근동맥의 근원성 반응은 정상과 비슷하게 유지되었다. 또한 $VOCC_L$ 전류 및 TRPC 전류, TRPC6 mRNA, Kv 전류, Kir 전류 모두가 정상측 다리의 골격근동맥과 유사하게 기능 회복이 관찰되었다.

이상의 결과는 하지위축 시 예상되는 골격근동맥의 혈류역학적 자극 감소가 동맥평활근의 기능적 변화를 일으키는 것을 보여주었다. 또한, 직접 수축-이완 운동은 불가능하더라도, 지구력 운동에 의한 체순환 증가 효과만으로도 마비측 혈관 기능 회복이 일어나는 것을 평활근세포 수준에서 보여주었다. 이 연구결과는 신경마비 또는 거동 제한 환자에 대한 적절한 재활성운동이 가져오는 유익한 효과를 골격근동맥의 생리적 기전을 통하여 이해하는데 도움이 될 것이다.

주요어: 좌골신경, 근원성수축반응, 동맥평활근세포, 이온 통로, 운동 훈련

학 번: 2016-30781